Project No. 10-928

Fuel Performance Experiments on the Atomistic Level, Studying Fuel Through Engineered Single Crystal UO2

Fuel Cycle/Reactor Concepts

Dr. Eric Burgett
Idaho State University

In collaboration with:
Georgia Institute of Technology
University of Florida

Frank Goldner, Federal POC
Keith Jewell, Technical POC

NEUP Nuclear Energy University Programs
U.S. Department of Energy

Idaho State University

921 South 8th Ave. Stop 8060
Pocatello, ID, 83209-8060
Phone: 2028-282-2220
Email: burgeric@isu.edu

Fuel Performance Experiments on the Atomistic Level, Studying Fuel Through Engineered Single Crystal UO_2

Final Report

Jan 30th, 2015

[Intentional Blank Page]

Approved By:

_____

Dr. Eric Burgett, Idaho State University

_____

Dr. Chaitanya Deo, Georgia Institute of Technology

_____

Dr. Simon Phillpot, University of Florida

[Intentional Blank Page]

Table of Contents

Table of Figures

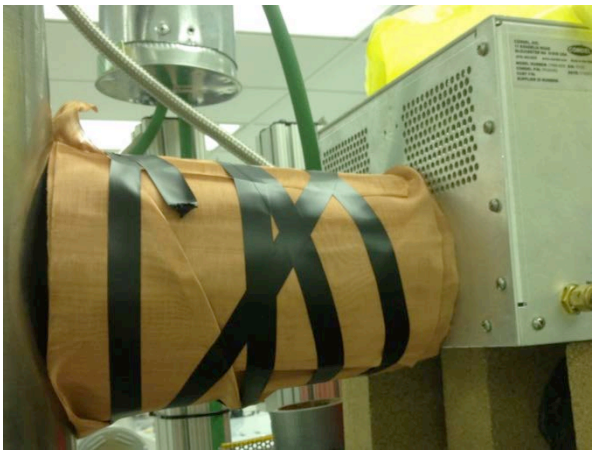

Introduction

The proposed engineered single crystal UO_2 program is designed to create custom engineered single crystal UO_2 samples for determining basic physical properties of UO_2 fuel. This program is led by an "Early Career Researcher" within the first 10 years of their academic career. Through custom engineered single crystals, phenomena such as fission product migration, fuel-cladding interactions, grain formations, grain propagation, heat transfer across grains can be studied in a controlled environment. The project will grow single crystals, as well as engineered crystals. The engineered crystals can consist of single crystals (grains) of UO_2, with fission product surrogate layers, as well as multi-grain systems with controlled grain boundaries. These studies combine state-of-the-art fuels modeling with unprecedented accuracy and precision experiments in a highly ordered system. By creating highly ordered engineered crystals, separate effects testing can be realized to generate high precision atomistic and macroscopic datasets. These datasets can be used to further enhance fuel cycle and reactor models. All of this work is in support of current and next generation fuel types for atomistic to macroscopic scale modeling efforts. This project is aimed at determining many of these fundamental physical properties in support of the FC R&D efforts.

The program will serve as a point for validation and verification of fuel performance simulation tools. These simulation tools employ methods at varying length and time scales. Using highly precise characterization tools, the atomistic properties of UO_2 will be measured, as well as fission product behavior, and grain mobility fuel used in current and new reactor designs. It is also possible to apply the same scheme to as well as cladding and structural materials in reactor based environments.

Three main physics parameters are will be studied; (i) the effect of grain boundary interfaces either within the fuel pellet itself; (ii) the physics of grain formation and propagation in various radiation, temperature, pressure, and atmospheric fields; and (iii) the physics of grain morphology, expansion, and reordering in these various radiation and temperature fields/gradients. These three physics parameters that are proposed to be studied are only the beginning of what could be investigated. Working with DOE, additional testing and parameters will be defined and studied.

These tests will require the development of a special nuclear fuel "oven" in which the coolant/atmospheric material, pressure, radiation source, and temperature can be changed in real time. The proposed "oven" will provide a unique opportunity to obtain information on the temperature atmospheric, radiation and pressure effects on single crystal fuel samples in real time measuring thermal expansion and grain formation and propagation. Quantifying these separate effects on defect migration will provide insight into the behavior of nuclear fuels. Since temperature and pressure are only two of the parameters that affect nuclear fuel behavior, the proposed oven will be designed in such a way that it can be easily integrated into a comprehensive separate effects testing capability in the future including gamma and neutron irradiation capabilities.

These four parameters will be investigated while working hand in hand with a strong physics modeling team in the proposal. Idaho State University, the lead university, will manage the crystal growth and fabrication methods. Georgia Institute of Technology and the University of Florida bring excellent atomistic modeling expertise, with University C also providing experimental facilities for characterization

of UO_2 single crystals. Researchers at the three universities will work hand in hand to design, model, and conduct the proposed experiments to create high fidelity data sets. In addition, the three university system will work with the national fuels campaign needs to create single crystal experiments that match their needs. It is intended to open the growth capabilities as a user facility, creating crystals as needed to support other research needs in the fuels campaign.

Current Status :

The project has wrapped up and is completed. It has met, albeit late, all of it's deliverables and milestones. The project has successfully grown large single crystals of uranium oxide, and tested them in several environments. These tests were modeled using KMC and MD simulations.

Deliverable #1 Commission new crystal growth facility for handling radioactive materials.

This will entail seeking appropriate radiation safety approvals which will start on day one. Prototype devices will be created from surrogate materials. A 6 month lead time on purchasing and arrival of hardware including AC Induction power supplies, cold wall crucible, reactor chamber, required MFCs and off gas processing components is anticipated. Estimated completion date of 4/1/2011. Installation will require roughly 3 months (7/1/2011). Commissioning time will be another 3 months (10/1/2011).

Milestone #1: Install and Commission new machine and obtain required RAM licensing. Completion date estimated at 10/1/2011.

Deliverable #1 (Participants) ISU

Deliverable #1 (Status) The Idaho State University Radioactive Materials License was amended to accommodate the requirements of the project. The amendment was awarded on August 3rd, 2012. ISU is now licensed to accept 200 kg of natural and depleted uranium metal and oxide.

The crystal furnace has been commissioned for a number of months, and has been growing surrogate crystals. Surrogate crystals were grown using the power supply, matching network, and furnace chamber. Examples are shown in Figure 1and Figure 2.

FIGURE 1 - MELT GROWN OF ND-DOPED YITTRIA STABILIZED ZRO2 CRYSTAL

FIGURE 2 – MELT GROWN CEZRO2 CRYSTAL

The crystal furnace power supply, high frequency matching network and induction coil have been successfully installed in the crystal growth lab. Further, the lift hydraulic system for crystal growth has been installed. A few samples of cerium (IV) oxide crystals were grown, and examined under a microscope and X-Ray Diffraction Analysis (XRD), results of those crystals and analyses are shown in deliverables 2. A number of tasks were required to finish commissioning crystal growth facility; where most of the pictures of those tasks are shown in **Appendices A**. Some of the major installations were:

- Water cooling system with specific pump requirements
- Water cooling temperature readouts (inlet and outlet temperatures)
- Pyrometer for oxide skin temperature readout
- Metal end caps for sealing furnace chamber
- Gas manifold for furnace chamber to run multiple gases
- Hydraulic pump and piston for oxide pellet lift motions
- Computer interface to include safety features

In order to grow bigger crystals (> 0.50 inches OD) using current high frequency matching network, some modification to the original matching network circuit had to be done. The original induction coil had a ¾ inch inside diameter (ID), 7 helical turn, and induction of 1.28 µH. In order to match that induction of 1.28 µH while increasing induction coil ID to 1-inch, number of helical turns had to go down by 2 turns as shown in Figure 3. The original matching network circuit had a limiting matching induction of 1.28 µH enabling to only fit up to 1-inch ID induction coil. A necessary modification was made to the matching network circuit enabling to fit up to 4-inch ID induction coil. Currently, the matching network uses a 2-inch ID induction coil with 7 helical turns and induction of 3.62 µH, as shown in Figure 4.

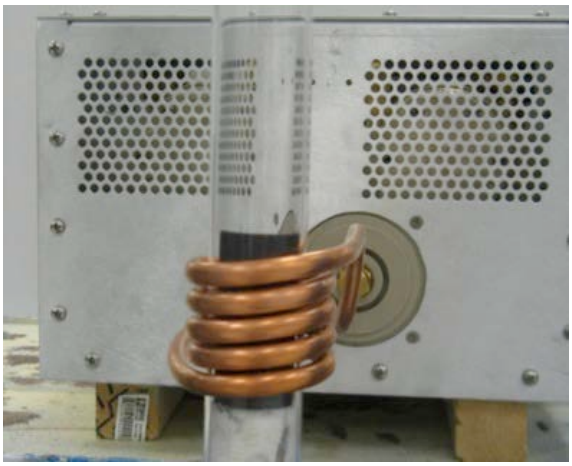

FIGURE 3 - 1-INCH (ID) INDUCTION COIL

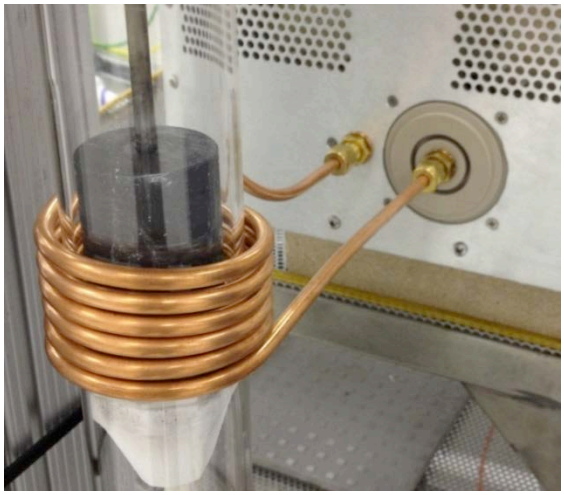

FIGURE 4 - 2-INCH (ID) INDUCTION COIL WITH GRAPHITE SUSCEPTOR

The crystal furnace is wired and plumbed to the cooling (primary) and emergency (secondary) water system (Figure 5). The inlet and outlet cooling lines from the matching network have attached temperature read-outs. Also, flow meter is installed on the inlet water-cooling line for further measurements of the system. Gas manifold system has been installed to flow primary forming gas (10% hydrogen and 90% nitrogen) through the furnace chamber to prevent graphite susceptor from oxidizing. However, the gas manifold system has additional gas lines such as argon, nitrogen and oxygen generator lines. Graphite susecptor is placed between glass quartz and oxide pellet for preheating non-conductive oxide pellet until molten phase is present (Figure 4). Both end caps, top aluminum and bottom stainless steel, have been attached to the furnace chamber for stability, and to seal the system (Figure 5). The hydraulic lift system uses hydraulic pump and piston for zone refining crystals. Also, working with very high temperatures between 2,500 °C and 3000 °C requires adequate safety equipment such as: welding gloves, welding masks/shields, welding coats, and safety glasses/sunglasses. Most of the furnace parts described above are shown in Figure 5, and much more details in **Appendices A**.

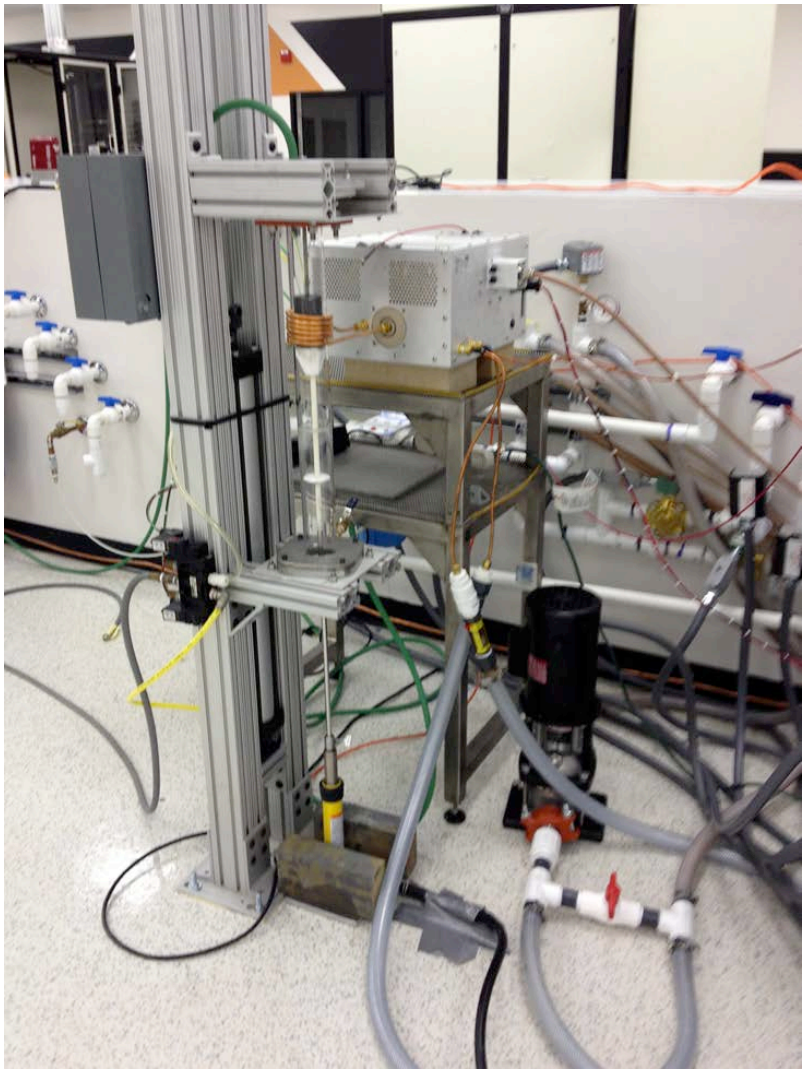

FIGURE 5 – HIGH FREQUENCY INDUCTION FURNACE

The 2-inch Induction furnace (Figure 5) was completed to accommodate growth of large bulk single crystals. All of the necessary equipment has been custom machined or pre-ordered. The completion date for pre-ordered equipment was 8/15/2012. Installation and machined parts required roughly a few weeks (9/15/2012). The 2-inch induction coil, quartz tube, steel/aluminum end caps, and specific Swagelok fittings were installed (Figure 5). The high frequency matching network has been modified to fit a bigger induction coil of up to 4-inch ID. This was accomplished by lowering the overall capacitance in the original circuit.

Induction furnace is controlled by a computer interface (**Error! Reference source not found.** & **Error! Reference source not found.**) that:

- Has interlock system for safety purposes
- Controls gas manifold system
- Controls power supply and matching network
- Reads real-time temperatures of:
  - Cooling water inlet
  - Cooling water outlet
  - Conductive material's skin temperature via pyrometer

Currently the graphical interface (Figure 6 & Figure 7) uses java syntax, where the code uses two modes for controlling power supply. The GUI mode allows you to control the values at the computer, where the script mode allows you to choose a file that is in an appropriate format ("recipe mode"). The GUI lets you use seek mode (Figure 6) or ramp mode (Figure 7) for controlling power supply. Ramp mode allows you to set maximum power, power/degree ramp up or down, and time step between each up/down ramp value. The seek mode allows you to choose maximum power, goal power or temperature, step size value, and time between steps. Finally all the data gets logged to the file name that gets entered at the beginning of running this interface code. The computer interface, and control box for the cooling system and power supply are shown in **Appendices A**.

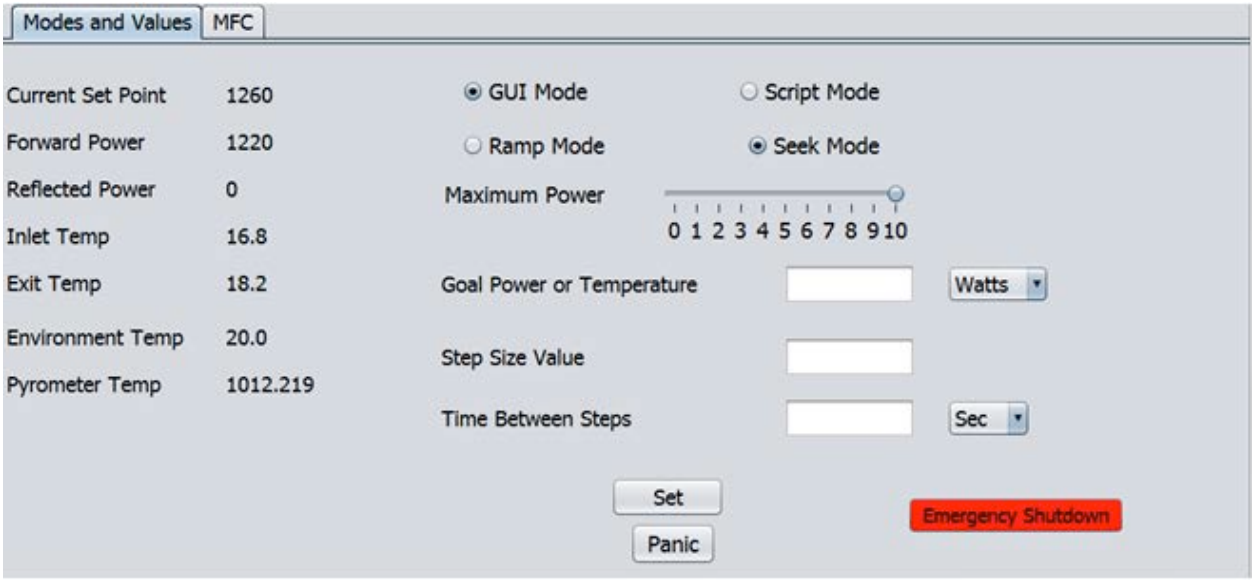

FIGURE 6 – COMPUTER INTERFACE: SEEK MODE

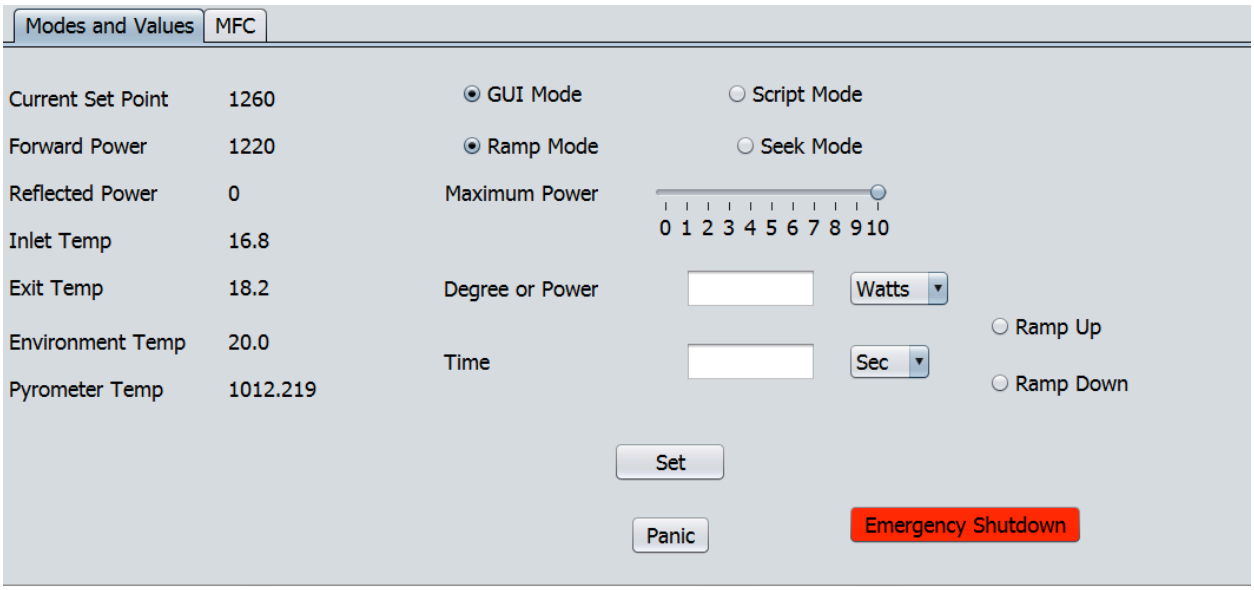

FIGURE 7 – COMPUTER INTERFACE: RAMP MODE

The process of making CeO_2 pellet requires three key components: laboratory scale, steel die, and specially designed sintering press. Care is taken not to contaminate the feedstock. The die is lubricated with a mixture of stearic acid and acetone followed by loading with the measured feedstock. Each pellet requires specific force applied depended on size of the pellet to achieve desired density. The required force to densify a ¾ inch outside diameter (OD) pellet is about 4,000 psi, which was repeated for about three times. Finally, the CeO_2 pellet gets taken out of the steel die gently using sintering press. This whole process is demonstrated in **Appendices A**.

A diamond wire saw and polisher system have been purchased (9/1/2012) and installed to cut and polish crystal samples (9/20/2012). Both machines are shown in Figure 8 & Figure 9.

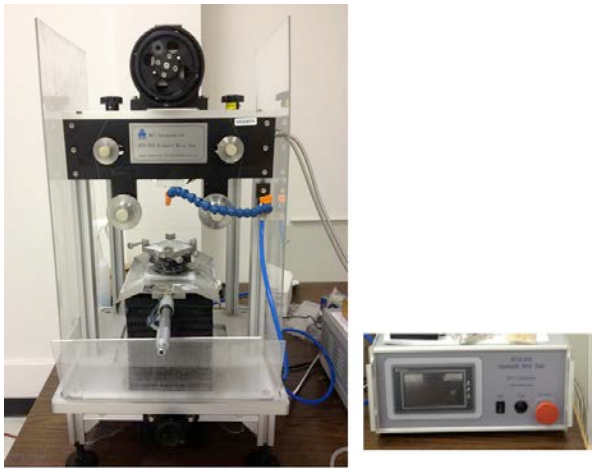

FIGURE 8 - HIGH PRECISION WIRE DIAMOND SAW

FIGURE 9 - AUTOMATED POLISHER SYSTEM

A new way of sintering pellets has been constructed using a 7-ton hydraulic ram (Figure 10), which could easily fit in the glovebox environment. New vertical sintering press works on hydraulic fluid making pressing charge pellet much easier. The 2 horsepower electric motor is designed for raw power, and has been put on the outside of glovebox environment for minimizing contamination..

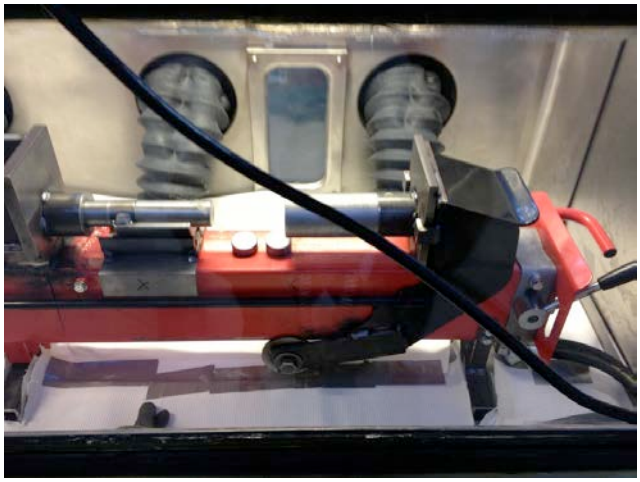

FIGURE 10 - MODIFIED HYDRAULIC RAM FOR PRESSING OXIDE PELLETS

In order to work safely with radioactive material, a glovebox was designed and installed. During the first quarter of 2013, a negatively pressured and double wall, stainless steel with lead core, glovebox has been designed and installed. The glovebox is in accordance with the American Glove Box Society Standard: AGS-G006-2005. This glovebox shell came prefabricated with an internal shell volume of 79 cubic feet, a 14-inch diameter antechamber, 12 glove ports and customizable feedthroughs for gas and wiring (Figure 11).

FIGURE 11 - FRONT VIEW OF THE GLOVEBOX

There are 6 glove port pairs on each side of the glovebox, with a sleeve and glove combo for easy glove change process (Figure 12). In order to eliminate pinch points (metal-to-glove contact) the gloves and sleeves were mounted with silicone and clamps. The glove and sleeve combo passed vacuum and leak tests multiple times. The windows are made of fire-resistant polycarbonate with channel-lock O-rings and bolt clamps. The antechamber is a two-door configuration with an independent vacuum and gas control system. The feedthroughs are located along the top and side of the glovebox with customizable wiring and plumbing systems.

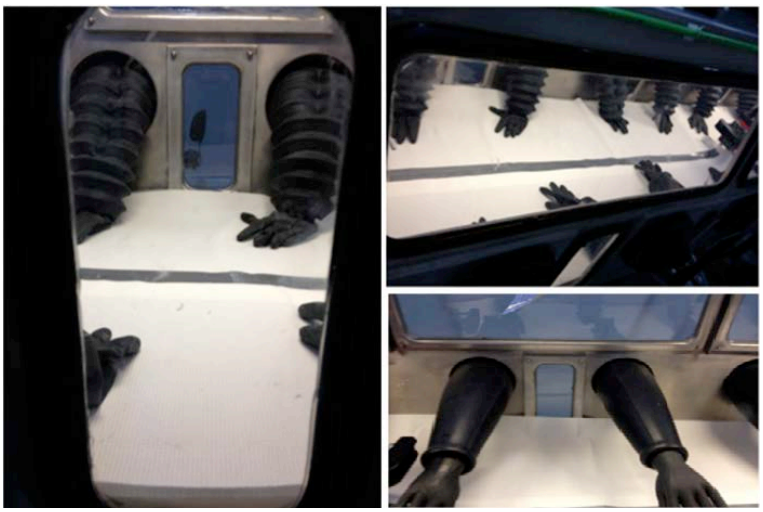

FIGURE 12 - THREE DIFFERENT VIEWS OF THE GLOVEBOX WINDOWS WITH GLOVE & SLEEVE COMBO

The electrical system can support equipment with 250V 20A, 3P 208V, 125V 20 A systems, and is shown in **Appendices A**. For further safety, the glovebox shell has been grounded. The internal emergency lighting is comprised of hermetically sealed LED lighting with separate 125V service, with battery backup. The external lighting consists of three fluorescent lights on top of the glovebox, with direct light falling through the windows.

The alarm system has two independent systems, smoke/heat detector and alpha particle isolation valve shown in **Appendices A**. The smoke/heat detector is a non-standard detector due to the high radiation environment in the glovebox. The detector is located in the center of the glovebox, and also connected to audible and visual alarm with a panel dialer. Further, the glove box alarm system has spark arrestor on vacuum line. The alpha particle isolation valve is set for precaution against contamination; therefore, installed post-HEPA filter. The main goal for the valve is to close the vacuum valve isolating the glovebox.

The plumbing systems consist of four different systems; shown in **Appendices A**. They are the vacuum system, inert gas system, monitoring system, and hydraulic system. The vacuum system has 1-inch diameter pipe going into the glovebox with one-way control valve to prevent over-pressurization. The inert gas system has 99.95% pure nitrogen (N_2) gas flowing through a 0.5-inch diameter feed at 70 psi. The flow is regulated with one-way control valve to also prevent over-pressurization of the glovebox. The monitoring system has a visual manometer reading of the internal pressure of the glovebox which is controlled by the adjustable inert gas.

The hydraulic system has the quick connects for supply and return hydraulic lines for the vertical pellet sintering press. The filter vacuum exhausts system has a drum HEPA filter, a secondary filtered diaphragm vacuum pump for a sampling loop along with a secondary one-way HEPA filter between two vacuum pumps. Finally, a small one-way HEPA filter inside the glovebox was installed to prevent backflow of gases. Table 1 illustrates the comparison of the AGS standard and the work completed on the glovebox, and more details are shown in **Appendices A**.

TABLE 1 - COMPARISON OF AGS STANDARDS TO GLOVEBOX DESIGN

Standard Requirement	Design
GB shell material and integrity	316 SS frame on 8 carbon steel supports
Gloves for boundary integrity	Butyl hands on neoprene sleeves
Gas filtration	HEPA filters (inlets & outlets)
Penetrations on removable plates	Several small removable plates
Shielding, if required by process	Double wall SS w/ lead insert
Pressure controls	Once-through flow w/ dampers and proper filters
30-ft candles of lighting	Interior LED, and exterior fluorescent
Fire protection based on process	Smoke/heat detector
Alarm displays and controls	Pressure, alpha, fire displays
Positive pressure decay test	Conducted by ISU-TSO
Face velocity test	Conducted by ISU-TSO

The crystal furnace has been updated to handle radioactive materials. The high frequency induction furnace that accommodates radioactive materials has been first designed in SolidWorks (**Appendices A**) and then custom machined on-site (Figure 13). The design consists of stainless steel (SS) body with build-in water jacket for constant cooling and shielding during growth process of a radioactive crystal. Further, the crystal furnace has two (2) windows of 4-inch diameter quartz plates for visibility. The original furnace chamber consisting of quartz tube, two metal end cups, two supporting metal plates, and 2-inch induction coil have been moved inside SS body with an additional stand; where it has uses four (4) 0.5-inch nylon threaded rods and two think metal plates. More details can be found in **Appendices A**.

The top plate of updated crystal furnace has process (furnace chamber) and shroud (between SS and process chamber) gas systems. The process gas system is for the original crystal furnace setup, and the shroud system is for cooling the SS containment. Process gas line uses original gas manifold to flow mainly nitrogen or argon gas into quartz furnace chamber. Vacuum pump is plugged directly into process gas exit (pulls gas from top of the quartz assembly) where uses exhaust system at the roof. A gas processing system onsite, once available, will replace exhaust system in the roof. The third port in the back of SS containment is for induction coil connection into matching network, which had to be insulated with fiberfrax and linerless rubber splicing tape from any arching issues during growth process. The build-in water jacket is constantly cooled with filtered water as well. More details are shown in **Appendices A**.

FIGURE 13 - INITIAL RADIOACTIVE MATERIAL'S CRYSTAL FURNACE

Final changes for the updated crystal furnace that handles radioactive material (Figure 14) have been completed and shown in **Appendices A**.

- Added HEPA filter on Vacuum pump
- Converted exit process gas (out of quartz furnace) hose to stainless steel
- Installed LED lights inside the crystal chamber's window
- Insulated four nylon and metal tubes with fiberfax

FIGURE 14 - FINAL VERSION OF RADIOACTIVE MATERIALS CRYSTAL FURNACE

The process of making UO_2 pellet includes five key components: glovebox environment (Figure 11), hammer-mill (**Appendices A**), laboratory scale, steel die (**Appendices A**), and specially designed sintering press (Figure 15). UO_2 fuel pellets are made very similarly to the CeO_2 process with few modifications. In a glovebox environment UO_2 feed stock material is crushed into very fine powder using the hammer-mill. Following by sieving fine UO_2 powder and performing a particle size analysis. Next, that material is placed in a graphite-sintering crucible and pressed into desired density. More details is shown in **Appendices A**.

FIGURE 15 - SPECIALLY DESIGNED SINTERING PRESS FOR UO_2 MATERIAL

A 1600°C tube furnace is used for sintering UO_2 pellet (Figure 16) before crystal growth to densify the powder even further and for annealing CeO_2 after the crystal growth. Both furnaces are shown in **Appendices A**.

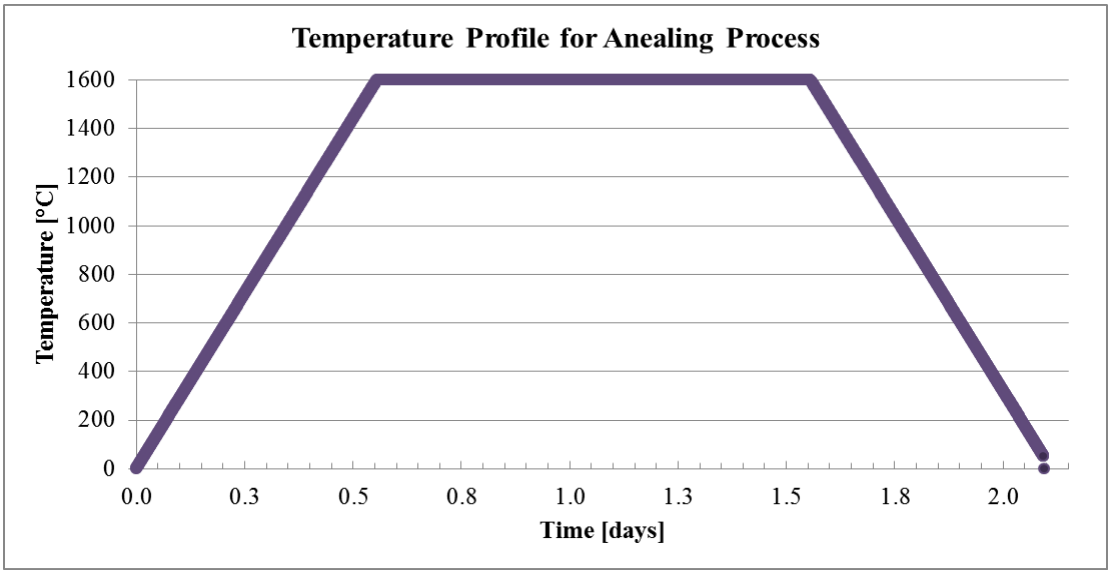

FIGURE 16 - TEMPERATURE PROFILE FOR ANEALING/SINTERING UO_2 PELLET

A design of new crystal furnace with glovebox assembly is in the process of finalizing before sent off to fabrication. The design is shown in Figure 17 as a 3D SolidWorks drawing. The idea behind this design was to build glovebox assembly around the induction furnace. The inner shell is made out of 11 gauge stainless steel and outer shell out of 16 gauge stainless steel (SS); between those two metal sheets a constant flow of cooling water in place for safety purposes. The design will use ten 7-inches by 10-inches lead glass windows. The new glovebox furnace has ten glovebox ports, which will use same sleeve/glove set-up as the on-site glovebox configuration. The upper part of the glovebox will be specifically for loading/unloading pellet into the induction furnace, which will include antechamber big enough to fit any quartz tube/assembly size used in growth process. Also, two large moving platforms were included in the design for loading materials in, adjusting proper heights, and other required positions. The final design will also consist of inner assembly for induction furnace, and lift & rotation of the pellet during crystal growth process.

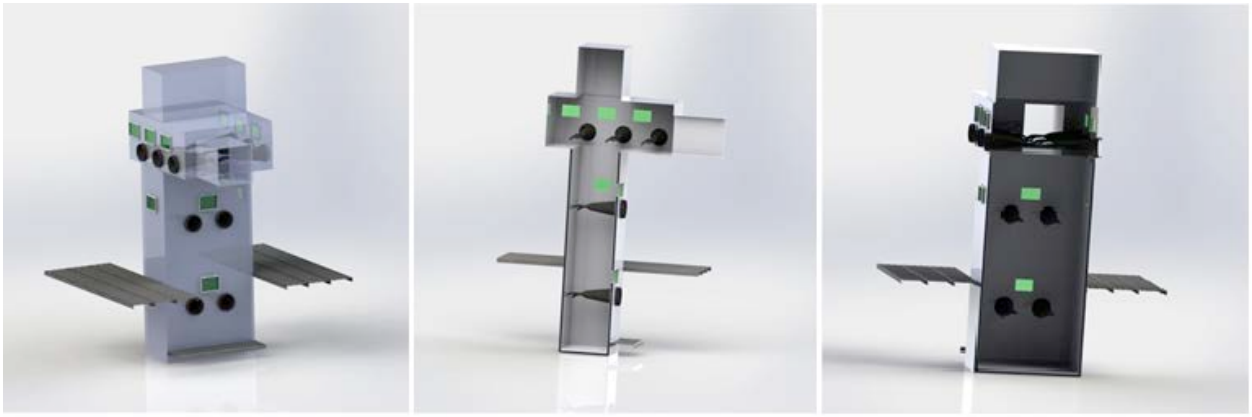

FIGURE 17 - SOLIDWORKS DESIGN FOR UPGRADED CRYSTAL FURNACE THAT HANDLES RADIOACTIVE MATERIALS

New crystal furnace has been installed and tested (Figure 18). The plumbing, induction coil, and power have been installed; it required power input of 380 V three phase 50 or 60 HZ, water flow of around 10 L/m, pressure of 0.2 MPa, and working water temperature between 20 to 35°C. The induction coil has been made out of 1-inch copper tubing with 6.5 turns; therefore, having inductance of 4.78 μH. High efficiency can be only achieved when proper adaption between power supply and turns of the induction coil is made. Heating time takes anywhere between 0.1 to 99.9 seconds. The whole installation set-up is shown in Figure 18 and **Appendices A**.

FIGURE 18 - 70 KW INDUCTION FURNACE FOR SINTERING OXIDE PELLETS

Since UO_2 gets crushed into fine powder with hammer-mill, the size and shape of those particles are not uniform. UO_2 "fluffer" system (Figure 19) has been design to uniform particle size and decrease overall density. Design was based on fluidized bed reactor concept, where it does chemical and physical process of the crushed UO_2 powder. First, UO_2 powders gets put into mild steel vessel, where the system will flow oxygen and heat to about 450 °C; this will oxidize the powder to UO_3. Next is to flow hydrogen and heat powder to even higher temperatures to bring UO_3 down to UO_2 form. All of this is controlled with a computer interface written in LabView; it has control over all the gas flows and temperatures.

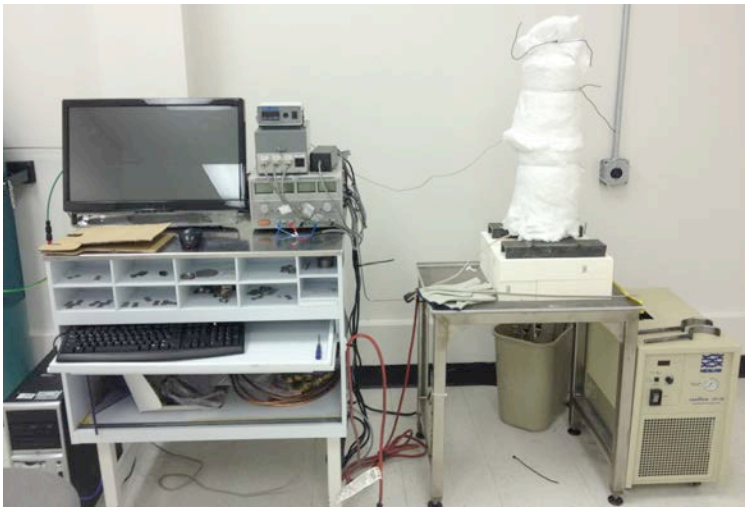

FIGURE 19 - URANIUM DIOXIDE "FLUFFER" SYSTEM

Deliverable #2: Grow single crystal uranium oxide.

This work will be done in conjunction with the efforts of National Lab. This project will work synergistically with National Lab to supplement their growth capabilities to provide the largest suite of available materials. Timeline to grow first crystal is 6 months following commissioning of new machine. (4/1/2012) Cutting, polishing, grain orientation and stoichiometric verification will take 3 months for the first sample (7/1/2012). Growth will continue for the duration of the project based on availability of feed stock materials.

Milestone #2: Grow, process (Cut/polish), and characterize the first single crystal bulk sample. Estimated completion date of 7/1/2012 growing surrogate Ceria samples with great success. The project has the required radioactive material licensing to take possession of the required uranium oxide precursor.

Deliverable #2: (Participants) ISU

Deliverable #2: (Status) Complete. The full power supply has been purchased, installed, commissioned and is operational. While Uranium Oxide has been shipped, it cannot be grown at this time. Cerium surrogate samples are shown below. Quality assurance documentation is being created for that instrument. No further work can be done on this task at this time. This deliverable will be impacted and pushed past its due date without a secured feedstock of materials which was outlined in the proposal. DOE is responsible for determining a source of this material. A source of these materials is still needed.

The first few runs were to adjust the right amount of power, cooling water flowrate, oxide skin temperatures via pyrometer, and timing. Once all the system parameters were set, a few sample crystals were grown as shown in Figure 20 and Appendices B. Columnar grain structures were desired from a rapid cooling of the sample. These columnar grain structures can be found in Appendices B. In addition, bi and tri-crystal structures were grown and are shown in Figure 21& Appendices B.

Figure 20 shows large bi- and tri-crystal interfaces prior to cutting and polishing. Light regions on the top are perfect stoichiometry; more red color regions to the bottom right of the Figure 20 are oxygen deficient at a ratio of 1:1.92.Cracks seen are separate crystal interfaces which have separated from the primary boule.

FIGURE 20 - LARGE CeO_2 BI- & TRI-CRYSTAL INTERFACES (AFTER ANNEALING AND PRIOR TO CUTTING & POLISHING)

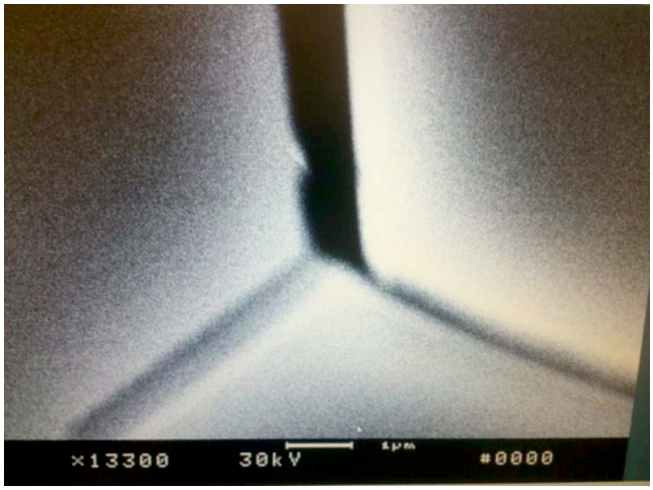

FIGURE 21 - SEM IMAGE OF CeO_2 TRI-CRYSTAL INTERFACE & CRYSTALLINE SEPARATION

X-Ray Diffraction Analysis (XRD) investigated crystalline material structure, including atomic arrangement, crystallite size, and imperfections for the cerium oxide crystals. The given results for cut and polished samples are shown in Figure 22. More Cerium (IV) Oxide crystals (Appendices B) have been grown with very good results (Appendices B). The 1.5-inch diameter 3-inch height cerium oxide pellet was cooked to about 1200 °C on the skin temperature and very slowly (3-5 °C every minute) cooled until the sample no longer coupled to the induction coil. The easy way of telling when the sample no longer couples to the induction coil is when the difference in temperature between inlet and outlet cooling water lines is greater than 5-10 °C. Once the ceria crystals were annealed in the material-processing oven (**Appendices A**), thin wafers of 0.1 mm were cut with the wire diamond saw and polished with automated polisher (Figure 8 & Figure 9 & Appendices B).

The X-ray diffraction analyses show very defined and smooth peaks (Figure 22) with peak [311] of 104.4 arcsec full width half max (FWHM) (Appendices B).

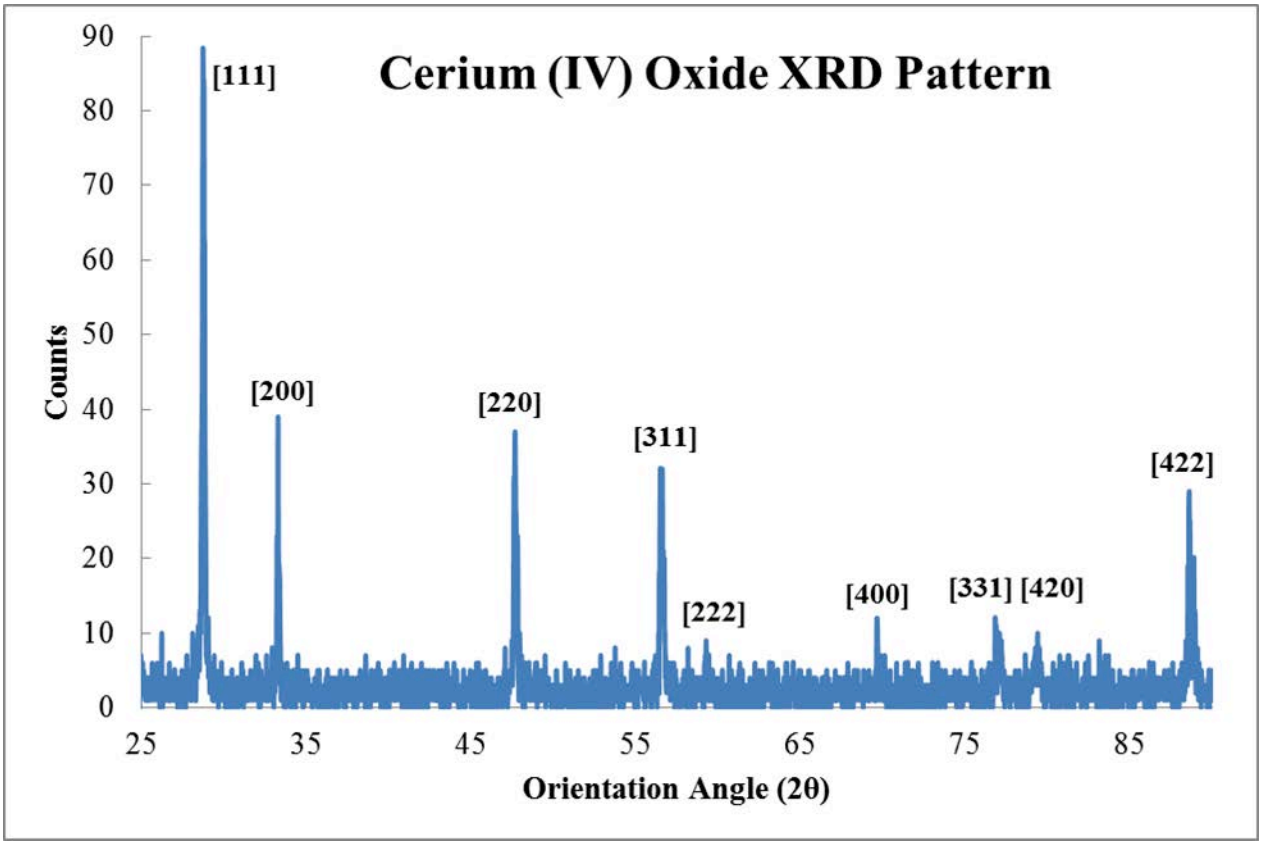

FIGURE 22 - XRD SPECTRUM OF CERIA CRYSTAL FROM 03-11-13 RUN

Uranium oxide has been stored in a nitrogen atmosphere for over 30 years, therefore, it is a difficult process to compress a solid uranium oxide pellet without having it to fall apart. At the beginning of this process, it was logical to press uranium oxide using the same process employed with surrogate cerium oxide. A related challenge when performing this process are the limitations of having to work in a glovebox environment due to radioactive material. However, it was discovered that even with more force applied to uranium oxide powder it would crumble out of the steel die. The next attempt involved using graphite pucks (**Appendices A**) at the bottom and top of the steel die, to encapsulate uranium oxide powder. Unfortunately, the uranium oxide was still able to crumble out of the steel die. The final, successful process used a graphite sleeve with two graphite pucks (**Appendices A**), one at the bottom and top of the graphite sleeve. The applied force was about 6,000 psi and held for about 15 to 30 minutes for the 1.5 –inch diameter pellet (this includes the graphite sleeve's diameter). Further, a graphite crucible was made to double encapsulate uranium oxide pellet for pre-cooking in a 1200 °C tube furnace (**Appendices A**). The pre-cooking process took about 6 hours at steady 1050 °C temperature, followed by removal of graphite crucible and graphite sleeve in the glovebox. Next, the uranium oxide pellet has been placed in the induction chamber and brought slowly to molten phase as previously with cerium oxide growth process. However, uranium oxide melts at much higher temperature (~3200 °C) and is a semi-conductor (as opposed to cerium oxide being an insulator). Process nitrogen gas (7 Lpm) was only used

during pre-heating process with the graphite susceptor in the induction chamber. Once the susceptor has been lifted, an argon gas replaces all of the process nitrogen gas (7 Lpm) and additional process oxygen gas (0.5 Lpm) has been added. A slideshow of UO_2 crystal growth before lift/rotation motors were put in place are shown below in Figure 23.

FIGURE 23 – SLIDESHOW DURING UO_2 CRYSTAL GROWTH

The whole UO_2 crystal growth process consumes almost entire week -- from crushing fuel pellets with hammer-mill, sifting UO_2 fine powder, pressing and sintering UO_2 pellet, pre-heating followed by melting pellet to completely cooling finished crystal.

Finally, a uranium oxide crystal has been created and is waiting for further analysis (XRD analysis/SEM imaging) as shown in Figure 24. The graphite sleeve used to successfully create a uranium oxide pellet resulted in a smaller pellet than intended, therefore a new steel die (**Appendices A**) has been made to produce 1.5-inch diameter uranium oxide pellet. Using this new steel die, the next uranium oxide pellet has been made and pre-cooked in the tube furnace over a whole entire weekend at 1050 °C (about 52 hours). The next step will be to grow a uranium crystal in the induction chamber, where the size of current pellet is 1.5 inches in diameter by about 4 inches tall. Further, 1200 °C tube furnace has been replaced with 1600 °C tube furnace for even better quality crystal of UO_2.

FIGURE 24 - URANIUM OXIDE CRYSTAL FROM DIFFERENT ANGLES

Few thin wafers of UO_2 have been cut with the diamond wire saw. Those wafers averaged about 0.125-inch of thickness and in 0.5-inch diameter. The Focused Ion Beam (FIB) microscope has been used to image some of first UO_2 samples (Figure 25) as well as for milling the top surface for polishing (Figure 26 & Figure 27). As shown in Figure 25 UO_2 crystal has few single crystals as well as few bio- and tri-crystals. Further, necessary single crystal x-ray diffraction analysis will be done for all of the UO_2 crystals in order to improve the current UO_2 growth.

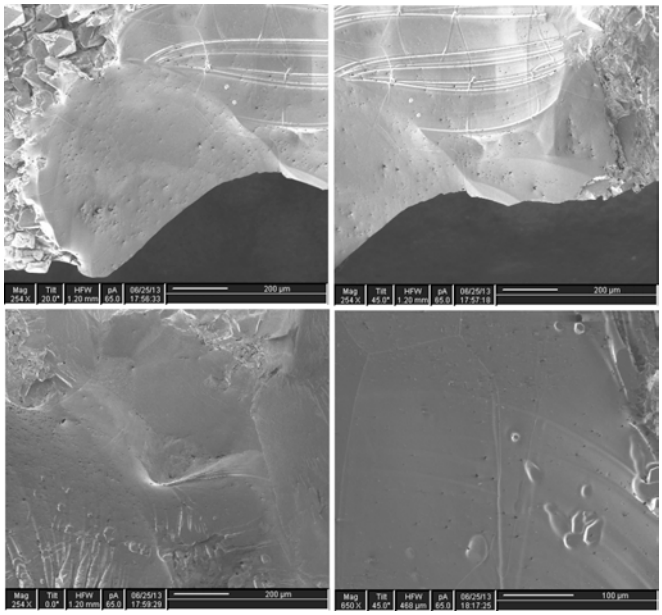

FIGURE 25 - FIB IMAGES OF VERY FIRST UO2 CRYSTAL SAMPLE.

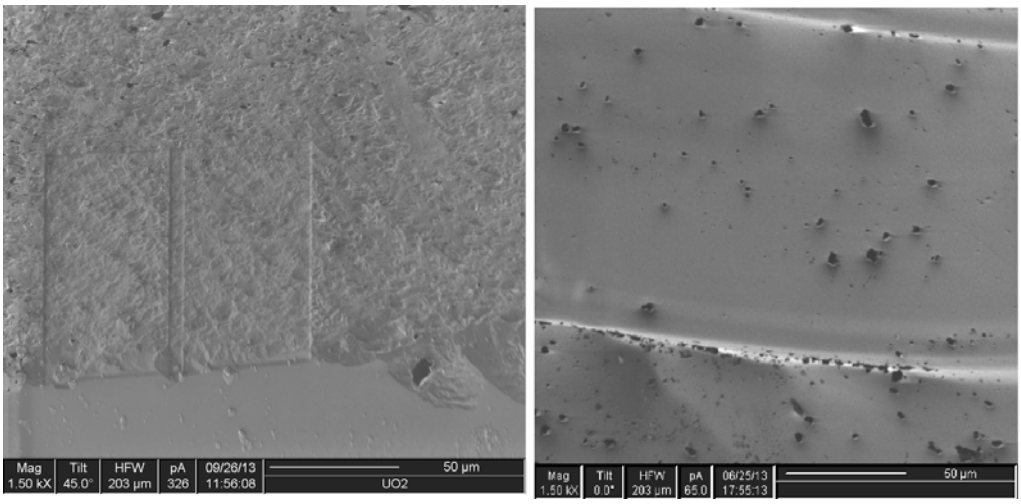

FIGURE 26 - FIB IMAGES OF MILLING THE TOP SURFACE OF UO2 DOWN

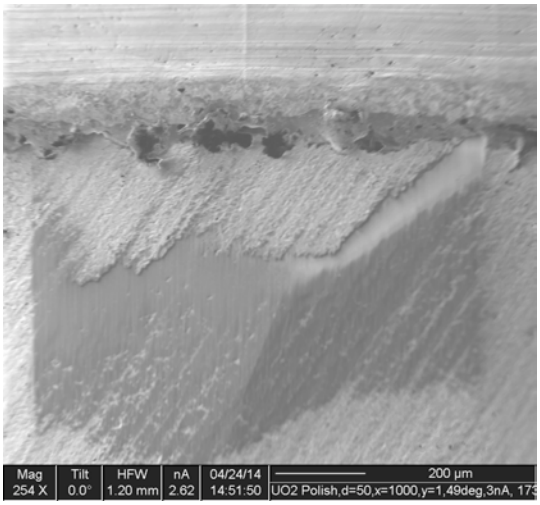

FIGURE 27 – TILTED FIB IMAGE OF POLISHED UO_2 CRYSTAL (TRI-CRYSTAL INTERFACE)

More UO_2 pellets have been made in the glovebox and pre-cooked in the 1600 °C annealing tube furnace. Finally, stepper lift & rotation motors have been implemented into growth process (**Appendices A**). The results of UO_2 crystal growth are shown in Figure 28 – UO_2 crystal grown with lift & rotation motors in place and Appendices B.

FIGURE 28 – UO_2 CRYSTAL GROWN WITH LIFT & ROTATION MOTORS IN PLACE

The deliverable is complete. Crystals were grown successfully.

Deliverable #3 Commission new MOCVD/CVD/ALD hybrid system for handling radioactive materials.

This task involves obtaining the appropriate radiation safety permits and installing the system. . Timeline to grow first MOCVD/ALD crystal is 6 months following the grown of the bulk crystal.

Milestone #3: Grow first layers of fission product surrogates on urania crystals. Estimated completion date of 4/1/2012.

Deliverable #3 (Participants) ISU/INL

Deliverable #3 (Status) Completed with alternative options. As an alternative option, a thermal and electron beam evaporator system has been purchased from another project in concert with INL. This device however was shipped by INL and damaged in shipment. This device will need to be replaced and funding to replace the item has yet to be identified in this fiscal year's budget. Lastly, a series of vacuum sputter deposition systems have been installed as a last resort. These units are being commissioned to deposit various metals such as gold, silver, silicon, germanium, and gadolinium. A functional sputter coater was commissioned this month and gold has been successfully deposited. Images of the system in cold standby can be seen in Figure 29, Figure 30, Figure 31, and Figure 32. To reiterate, no progress can be made on commissioning the MOCVD tool until the remainder of funding is distributed to ISU for the remainder of the support infrastructure. The thermal and electron beam evaporator cannot be completed, repaired, and installed until INL/BEA distributes funding to replace the power supply which was broken by their shipping agency.

The team got the gas lines ran, the crystal furnace fully functional, some cerium oxide crystals grown, and the MOCVD machine is very close to becoming fully functional.

- Set up the air showers in the MOCVD room
- Ran the Oxygen and Nitrogen lines to the MOCVD
- Ran the Green line for the MOCVD and got it plumbed in for the nitrogen generator.

- Helped Dee set up the air showers in the MOCVD room
- Also starting to work with the welder again and getting it set up for the MOCVD lines
- Have assisted Dee in getting the small bellows for the MOCVD and the large tubing also.
- Ran the Green line for the MOCVD and got it plumbed in for the nitrogen generator.
- Ran the nitrogen lines for the MOCVD

FIGURE 29 - PHOTO OF THE MOCVD TOOL BEING INSTALLED AT THE RISE COMPLEX

FIGURE 30 - IMAGE OF THE MOCVD CONTROLLER UNIT DURING THE INSTALLATION AT THE RISE COMPLEX

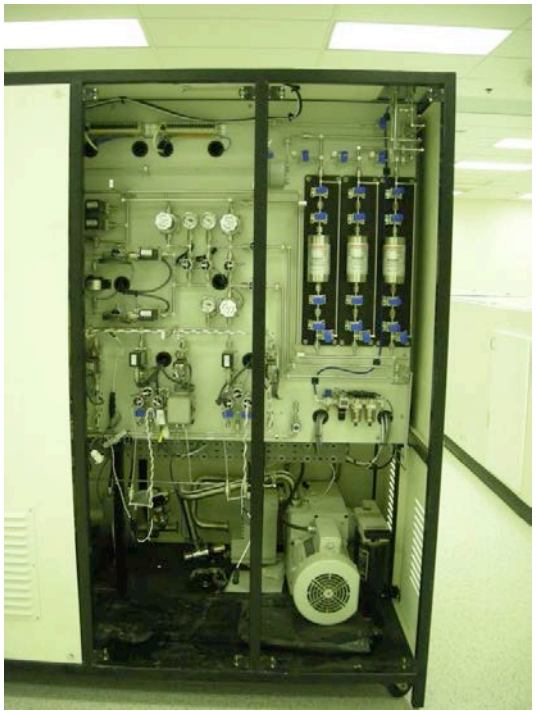

FIGURE 31 - IMAGE OF THE BACK SIDE OF THE MOCVD TOOL DURING INSTALLATION AT THE RISE SHOWING THE SEVERE DUTY VACUUM PUMP

FIGURE 32 - POWER SUPPLY AND CONTROLLER UNITS TO THE THERMAL AND E-BEAM DEPOSITION TOOLS

This quarter we replaced old pipes in the MOCVD (Metal Oxide Chemical Vapor Deposition) machine in preparation for activation. We have started figuring out how to remotely control the CX10K inductive heater. The two rapid thermal anneal furnaces have been inspected and are ready to be connected to power supplies. The crystal growth clean room has been partially cleaned and in preparation for becoming an active clean room.

The major update for this quarter was in the last days of the quarter, we received the uranium oxide feedstock in pellet form from the INL. We will begin to work on crushing the pellets into powder and then re-sintering the pellets in preparation for growth in the crystal furnace.

Completed.

Deliverable #4 Grow engineered single crystals of Uranium oxide with fission product materials.

This task will grow the bulk of the samples used in this project. Cutting, polishing, grain orientation and stoichiometric verification of the first samples will take 6 months for the first sample. (10/1/2012) Growth will continue for the duration of the project based on availability of feed stock materials. This will start simultaneously as Task 3.

Milestone #4 Grow and characterize the first MOCVD grown engineered crystal sample. (10/12/2012)

Deliverable #4 (Participants) ISU/INL

Deliverable #4 (Status) Completed.

Engineered crystals were grown with surrogate fission product materials including zinc, aluminum gold, and other metals and oxides. These materials were in diffused as well as discrete layered forms.

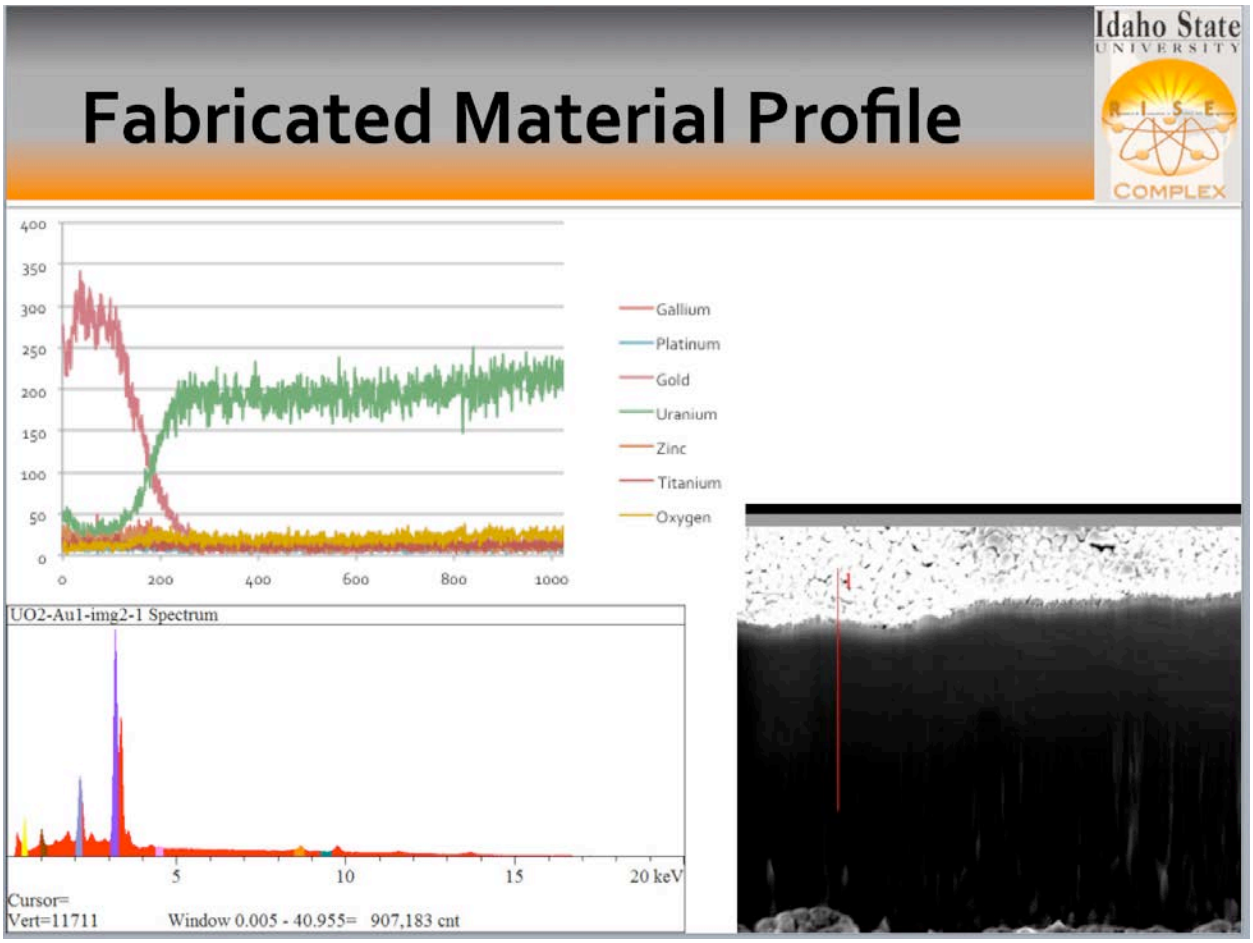

FIGURE 33 FABRICATED ENGINEERED CYRSTAL SHOWING LAYERED DEPOSITIONS AND SURROGATE FISSION PRODUCTS.

Deliverable #5 Commission multi zone fuel furnace.

This will entail obtaining the correct radiation safety permits and constructing the device.

Milestone #5: Commission new fuel furnace. Estimated completion date of 10/1/2011.

Deliverable #5 (Participants) ISU/Consultant

Deliverable #5 (Status) The unit has arrived at ISU and is now located in the RISE. The unit has been tested in atmosphere up to 900 °C. The design of the furnace tube, gas handling system, neutron source, photon source and positive ion source has been completed. See Figure 34, Figure 35, Figure 36, Figure 37, Figure 38, Figure 39, and Figure 40 below for the delivered multi-zone testing furnace.

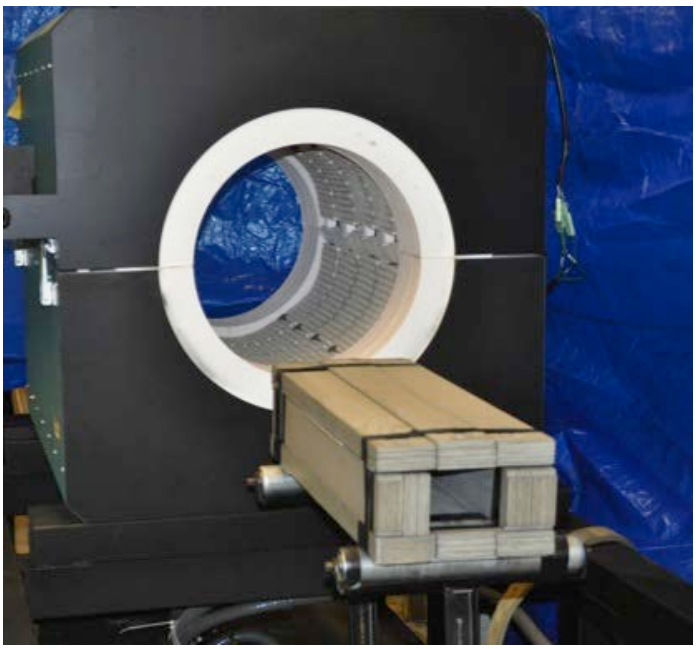

FIGURE 34 - MULTI-ZONE TESTING FURNACE WITH MOCKUP OF URANIUM FUEL NEUTRON BOOSTER FROM THE ISU SUBCRITICAL ASSEMBLY

Work this quarter progressed to include the installation of the atmospheric testing chamber into the multi-zone testing furnace. This thick-walled stainless steel pressure vessel was installed without its end caps. The furnace will be wrapped with insulation this quarter for safety. This furnace has again been tested to 900 °C with an open, air filled configuration. End caps will be created next quarter with viewing ports for line of sight access during irradiation. This can be seen Figure 37. A lower temperature box furnace with atmospheric control has also been procured. This lower temperature furnace is capable of temperatures up to 300 °C for long term heated irradiation studies. This can be seen in Figure 38. To study the effect of transients on the fuel materials being grown, a pulsing high temperature furnace has been procured. It can be seen in Figure 39. This furnace is capable of rapidly pulsing it's temperature up to 2000 °C to study the effect of transients on the nuclear fuel in a comprehensive separate effects testing capability.

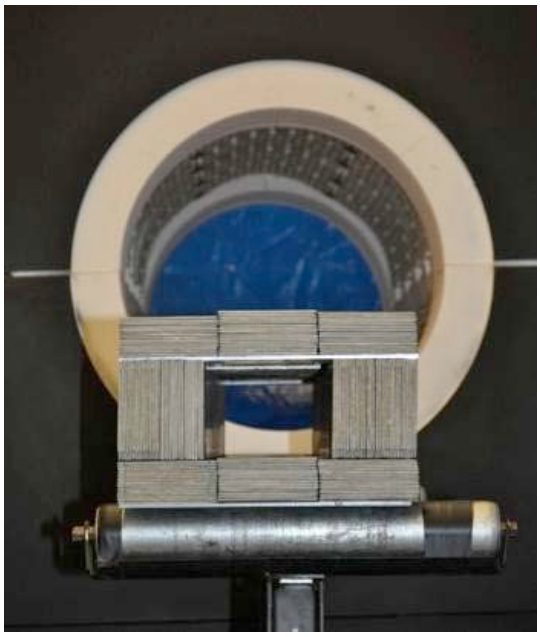

FIGURE 35 - MULTI-ZONE TESTING FURNACE WITH MOCKUP OF URANIUM FUEL NEUTRON BOOSTER FROM THE ISU SUBCRITICAL ASSEMBLY

FIGURE 36 - MULTI-ZONE FURNACE INSTALLED WITH ATMOSPHERIC CHAMBER INSTALLED

FIGURE 37 - MATERIALS TEST FURNACE WITHOUT END CAPS, OPERATING AT 1150 °C

FIGURE 38 - LOW TEMPERATURE BOX FURNACE FOR IRRADIATION AND HEATING OF SAMPLES

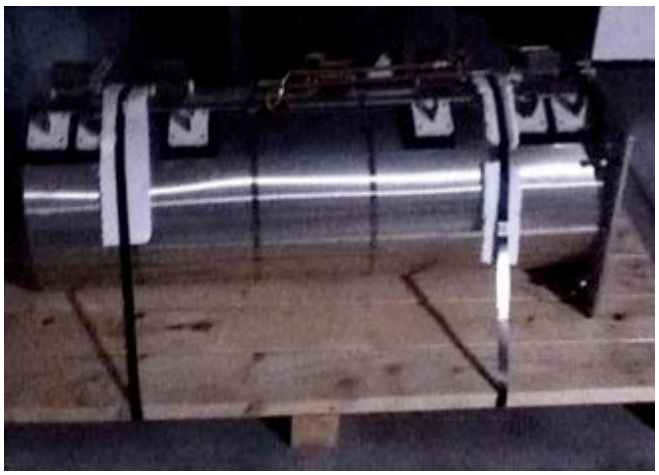

FIGURE 39 - NEW RAPID PULSED TESTING FURNACE FOR STUDIES OF TRANSIENT SEPARATE EFFECTS TESTING

The D-D neutron generator has arrived this quarter and is intended to provide a fast neutron fluency rate of 10^8 n/cm^2/s. This neutron generator has begun to be tested and has been tested and shown to emit at least 10^8 n/cm^2/s. It's total neutron output has yet to be determined since it is still being commissioned and conditioned. The neutron generator can be seen in Figure 40.

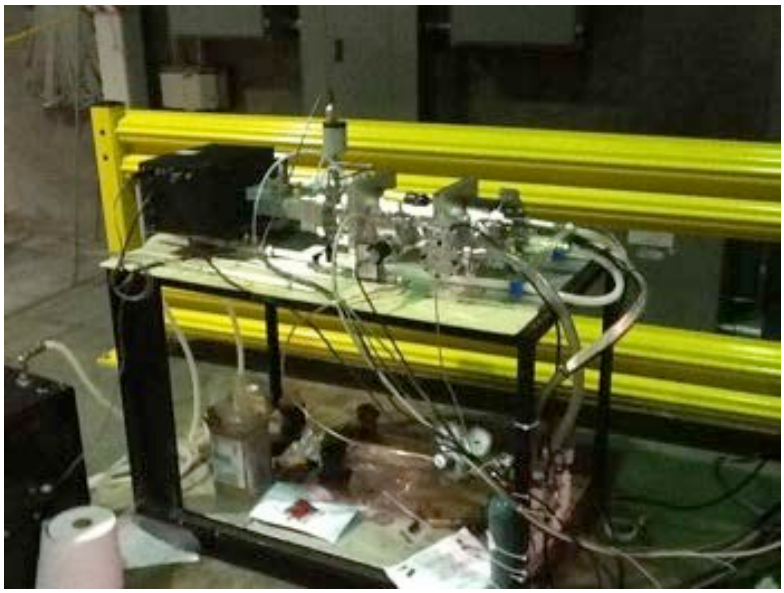

FIGURE 40 - D-D NEUTRON GENERATOR BEING COMMISSIONED AT THE RISE

Deliverable #6 Test new engineered single crystals.

This will include temperature studies, grain propagation/impact on various parameters. This will be conducted in the new fuel test furnace. This testing will begin when the first samples of bulk materials are prepared. Timeline to completion for first set of irradiation tests is 6 months. This testing will then run the duration of the project.

Milestone #6: Results from first round of irradiation tests will be collected. Estimated completion date of 1/1/2013.

Deliverable #6 (Participants) ISU

Deliverable #6 (Status) This quarter, the scanning electron microscope was installed in the new RISEfacility. Neutron and photon testing configuration modeling continues to optimize the irradiation geometries. Pictures of the delivered SEM are shown below in Figure 41, Figure 42, and Figure 43. In addition, the creation of Q/A standards has begun this quarter on the SEM. Shown below in Figure 44, Figure 45, Figure 46, and Figure 47 are a number of Q/A standards used to calibrate the SEM.

The positive ion irradiation high DPA source, a tandem pelletron capable of 9 MeV protons at up to 100 uA has been tested. The current operational limit of 1 uA is imposed due to dose rate concerns with the accelerator. This will provide adequate current and irradiation configurations for this project. The current accelerator can be seen in Figure 49 and Figure 50. This quarter an operational use permit has been filed for operation of the tandem pelletron (Figure 48) at high current, 200 uA, but at low energy, 1 MeV. This will allow for testing of samples at the end station.

FIGURE 41 - STUDENT WORKING ON THE NEWLY COMMISSIONED SEM AT THE RISE.

FIGURE 42 - PICTURES OF THE SEM AT WORK

This is a picture of the image resolution prickly gold Q/A standard. On the right is the EDAX x-ray spectrum of the image on the left showing the components in the sample. On the far right is the infrared chamber camera for monitoring the sample in the chamber.

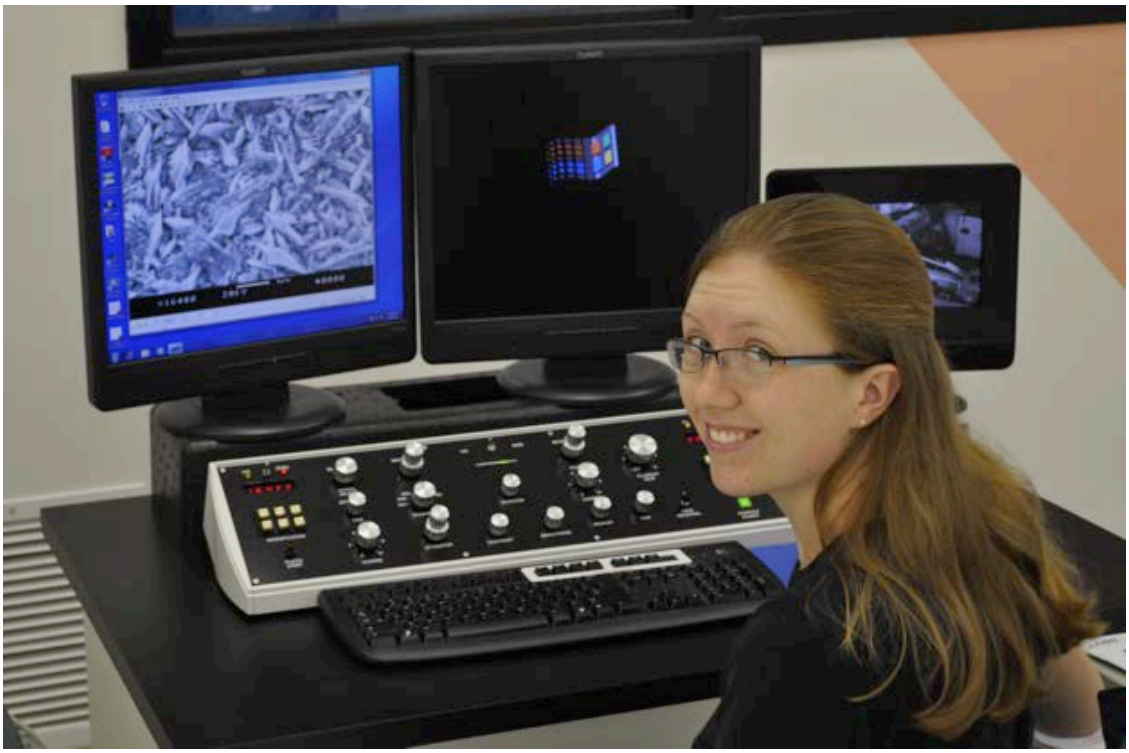

FIGURE 43 - HOLLY THORNTON USING THE NEWLY COMMISSIONED SEM

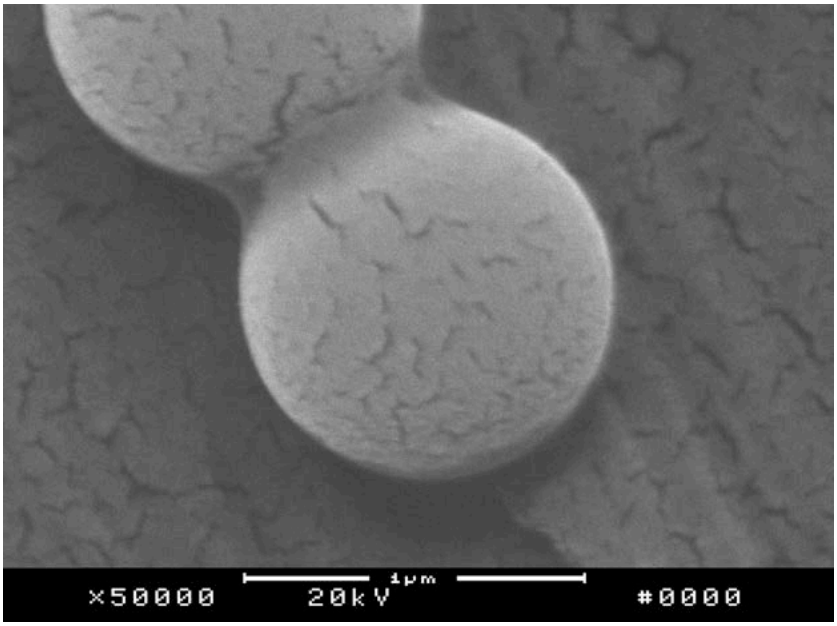

FIGURE 44 - ONE OF THE QUALITY ASSURANCE TEST SPECIMENS ON TWO LATEX SPHERES OF ONE MICRON SIZE IN THE COMMISSIONED SEM AT THE RISE

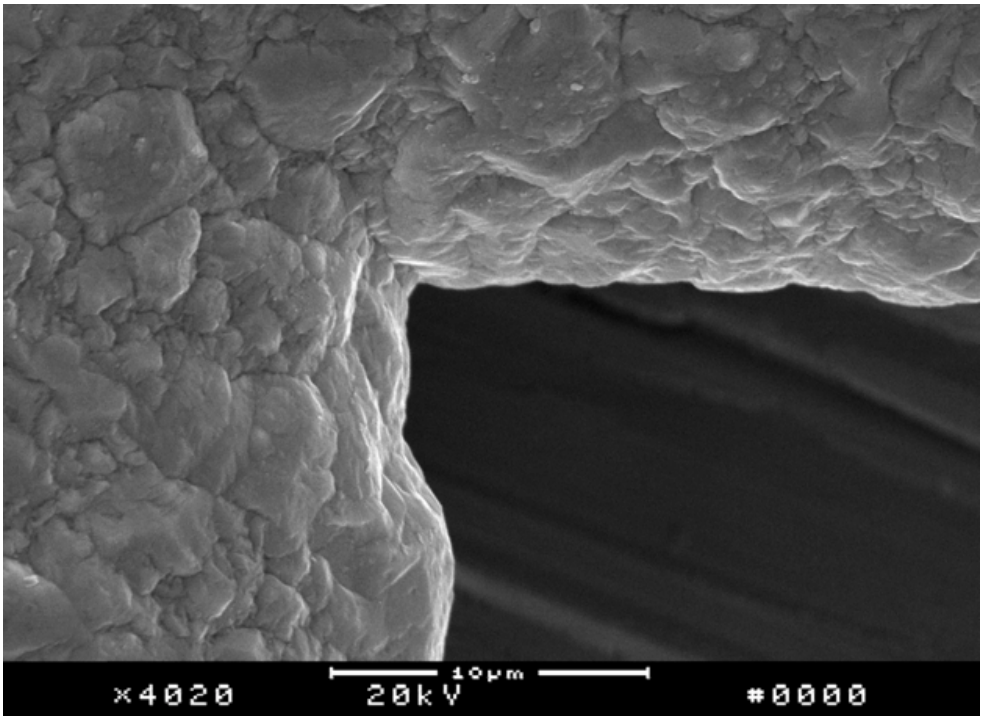

FIGURE 45 - SEM CALIBRATION GRID AND IMAGING RESOLUTION TESTING AFTER COMMISSIONING AT THE RISE

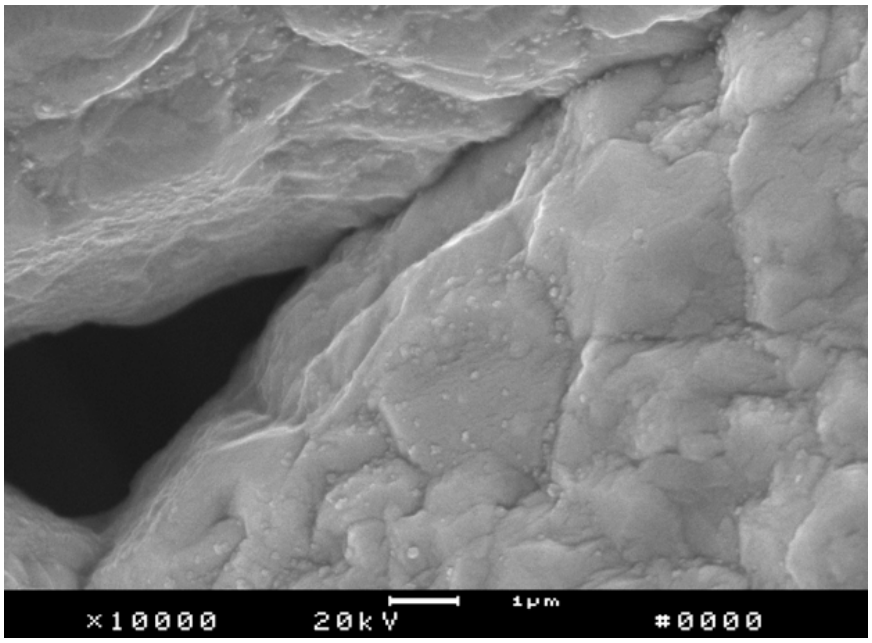

FIGURE 46 - SEM CALIBRATION GRID AND IMAGING RESOLUTION TESTING AFTER COMMISSIONING AT THE RISE. THIS FIGURE ILLUMINATES THE CRACK DEFECT RESOLUTION OF THE SEM

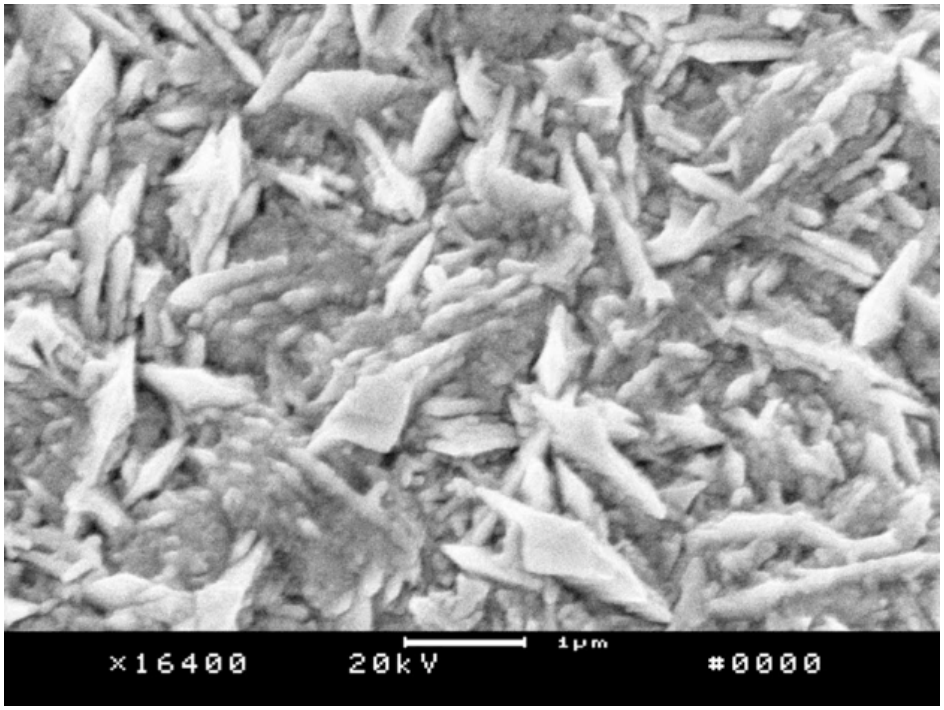

FIGURE 47 - PRICKLY GOLD IMAGE RESOLUTION Q/A TEST FOR THE INSTALLED SEM AT THE RISE

FIGURE 48 - TANDEM PELLETRON INSTALLED AT THE IAC

Additionally, a high power electron accelerator has been procured by ISU. This accelerator is a high resolution imaging and irradiation accelerator. This accelerator is currently being commissioned. It can be seen in Figure 49 and Figure 50.

FIGURE 49 - IMAGING ACCELERATOR BEING COMMISSIONED

FIGURE 50 - IMAGING ACCELERATOR BEING COMMISSIONED (2ND VIEW)

Completed.

Deliverable #7 Model and test results.

Guiding the program, Atomic Scale Modeling and Simulation of Defects and Fission Products in uranium dioxide single crystals will work in an iterative fashion with Task 6 to focus the effort to ascertain the best experimental data. Following the first true experiment, results will be compared to models. The timeline to first modeled results will be 3 months following the completion of the first tests.

Milestone #7: First models will be run simulating the first experiments. Estimated completion date of 4/1/2013.

Deliverable #7 (Participants) ISU, UF, GT

Deliverable #7 (Status) Several reports are being created for this deliverable. One summary is shown below on Molecular dynamics study of defects in uranium dioxide. This was completed.

Effect of Ce^{4+} and Th^{4+} Ion Substitution in Uranium Dioxide

Rakesh K. Behera[1], and Chaitanya S. Deo[1]

[1]Nuclear and Radiological Engineering Program, George W. Woodruff School of Mechanical Engineering, Georgia Institute of Technology, Atlanta, GA 30332, U.S.A.

ABSTRACT

Uranium dioxide is the most common fuel used in commercial light water nuclear reactors. The fission of the fuel generates fission products (FPs) and minor actinides (MAs), which affects the thermo-physical properties of the fuel. The understanding of the physical and chemical properties of

the FPs and MAs is still limited. In this study we have used atomic level simulations to estimate the effect of Ce^{4+} and Th^{4+} ions in urania matrix. Our results show that the structural variation depends on the elastic effect, which is guided by the ionic radius of the substituted ion. Ce^{4+} (ionic radius 0.97 Å) reduces the overall lattice parameter, while Th^{4+} (ionic radius 1.05 Å) increases the overall lattice parameter of the urania matrix (U^{4+} ionic radius 1.00 Å). In addition bulk modulus of the $U_{1-x}Ce_xO_2$ system does not change with substitution while the modulus of $U_{1-x}Th_xO_2$ reduces with an increase in Th^{4+} ion concentration. This observation is in accordance with Vegard's law prediction based on the modulus values of bulk UO_2, CeO_2 and ThO_2 systems.

INTRODUCTION

Uranium dioxide is the most common fuel used in commercial light water nuclear reactors. The fission of uranium based fuels in a light water reactor generates more than 20 fission products (FPs) [1]. In addition, the neutron capture and decay reactions during the fuel cycle produces minor actinides (MAs). These FPs and MAs affect the thermo-physical properties, e.g., thermal conductivity, swelling, creep of the fuel. Lanthanides and actinides are usually dissolved in the host UO_2 matrix. This paper studies the effect of these elements on structure and elastic constants of the host UO_2 matrix using atomistic simulations.

Considering the FPs and MAs, uranium-based fuels can generate Ce, Nd, Pm, Sm, Eu, and Gd in the Lanthanide series and Th, Np, Pu, Am, and Cm in the Actinide series. In this study we have investigated the structural and mechanical properties of UO_2 for 4+ ion (Ce^{4+} or Th^{4+}) substituted urania-systems using atomistic models. Atomic level simulations are successfully used to simulate nuclear materials [2]. In addition it is possible to define the substitution of the species of interest with atomic precision. Since we are interested in investigating the structural and elastic properties of UO_2 and substitution of Ce^{4+} and Th^{4+} in the urania matrix, we have collected relevant interatomic potentials from the literature.

METHODOLOGY

In order to simulate the urania systems with Ce^{4+} and Th^{4+}, we employ the transferable interatomic potentials from the literature which are described in table I. The overall interactions in urania systems are calculated by a combination of long-range and short-range interactions. The long-range interactions for all the potentials are described by the Coulombic interaction with Ewald sum.

$$V_{Coul}\left(r_{ij}\right) = \frac{1}{2}\sum_{i=1}^{N}\left\{\sum_{j\neq i}\frac{q_i q_j}{4\pi\varepsilon_0 r_{ij}}\right\} \quad (1)$$

Where N is the total number of ions in the system, ε_0 is the permittivity of free space, q_i, q_j are the magnitude of charges on ions i and j, and r_{ij} is the separation between ions i and j.

Table I. Interatomic potential parameters used to simulate Ce^{4+} and Th^{4+} ions in urania.

Species	Buckingham parameters			Core-shell parameters		
	A [eV]	ρ [Å]	C [eV·Å^6]	q_{core} [e]	q_{shell} [e]	k_2 [eV·Å^{-2}]
Grimes [3]						
$O^{2-} – O^{2-}$	9547.96	0.2192	32.0	0.04	-2.04	6.30
$U^{4+} – O^{2-}$	1761.775	0.35642	0.0	4.10	-0.10	160.00
$Ce^{4+} – O^{2-}$	1809.68	0.3547	20.40	4.20	-0.20	177.84
Nadeem [4]						
$O^{2-} – O^{2-}$	25.41	0.6937	32.32	0.513	-2.513	20.53
$U^{4+} – O^{2-}$	9296.65	0.2796	90.00	5.00	-1.00	134.00
$Th^{4+} – O^{2-}$	8638.50	0.2856	70.00	4.64	-0.64	110.00
$Ce^{4+} – O^{2-}$	7549.87	0.2831	70.00	2.75	1.25	222.00
Arima [5]						
$O^{1.35-} – O^{1.35-}$	919.17	0.332	17.36			
$U^{2.7+} – U^{2.7+}$	2.48 x 10^{+13}	0.072	0.0			
$U^{2.7+} – O^{1.35-}$	55918.39	0.202	0.0			
$Th^{2.7+} – O^{1.35-}$	31321.23	0.220	0.0			
Osaka [6]	Buckingham parameters			Morse parameters		
	A [eV]	ρ [Å]	C [eV·Å^6]	D [eV]	β_{ij} [1/Å]	r^*_{ij} [Å]
$O^{1.2-} – O^{1.2-}$	2346.1488	0.32	4.14616			
$U^{2.4+} – U^{2.4+}$	442.2081	0.32	0.0			
$U^{2.4+} – O^{1.2-}$	1018.5705	0.32	0.0	0.78101	1.25	2.369
$Th^{2.4+} – Th^{2.4+}$	17.0261	0.82	0.0			

$Th^{2.4+} - O^{1.2-}$	61.4295	0.57	0.0	1.21500	1.90	2.360

The short-range interactions, which are predominantly repulsive, are given by the Buckingham and/or Morse interactions. The Buckingham potential [7] is given as:

$$V_{Buck}\left(r_{ij}\right) = A_{ij}\ \exp\left(-r_{ij}/\rho_{ij}\right) - C_{ij}/r_{ij}^{\ 6} \qquad (2)$$

where r_{ij} is the separation between two ions i and j; and A, ρ, and C are free parameters. The Morse potential [8], which is used to describe the covalent bonding in the system, is given as:

$$V_{Morse}\left(r_{ij}\right) = D_{ij}\ \left\{\left[1 - \exp\left(-\beta_{ij}\left(r_{ij} - r_{ij}^{*}\right)\right)\right]^{2} - 1\right\} \qquad (3)$$

where r_{ij} is the separation between two ions i and j; and D, β and r_{ij}^{*} are free parameters.

The Grimes and Nadeem potentials are shell-model potentials whereas Osaka and Arima potentials are rigid ion models. In the shell model [9], each ion is described by a core and a shell, the sum of whose charges is the ionic charge of each species. A shell model where the core and shell of an atom are coupled by a harmonic spring is given by:

$$V(\omega) = \frac{1}{2}k_2\,\omega^2 \qquad (4)$$

where ω is the core-shell displacement, and k_2 is the harmonic spring constant. In the rigid ion model the ions are defined by point charges. The Grimes and Nadeem potentials are full charge models (Th^{4+} and O^{2-}), whereas Osaka and Arima are partial charge models.

The General Utility Lattice Program (GULP) [10, 11] was used to predict the structural and elastic properties discussed in this article. All the calculations were performed for a range of Ce^{4+} and Th^{4+} ion substitution with random distribution in the urania matrix (maximum 40% cation substitution). This distribution represents the solid solution condition as reported by Kleykamp [1]. A system size effect on the overall properties is performed and all the results presented in this article are based on a 4 x 4 x 4 super cell system.

RESULTS AND DISCUSSIONS

Before discussing the effect of Ce^{4+} and Th^{4+} ions in urania, it is important to analyze the bulk properties of UO_2 predicted by all the interatomic potentials. Table II lists all the elastic properties of UO_2, which is a re-calculation and summary of the data presented in the literature [2-6] and the references therein. The lattice parameter is predicted within 0.1% of the experimental numbers by most of the potentials, except Arima, which underestimates the lattice parameter by ~0.45%. The individual elastic constants are overestimated for Grimes, Nadeem and Arima; which is typical of interatomic potentials. Osaka is the only potential which underestimated the C_{12} and C_{44}. Hence, the bulk modulus of UO_2 is underestimated by ~12% for Osaka potential. In addition it should be pointed out that the experimental values are measured at a finite temperature while all the simulation results are calculated at 0 K.

Table II. Comparison of bulk properties of UO_2 calculated from different interatomic potentials with experiment.

	Experiment [2]	**Grimes**	**Nadeem**	**Osaka**	**Arima**
Lattice parameter [Å]	5.4698 [12]	5.4681	5.4749	5.4654	5.4449
Lattice Energy (eV/ThO_2)		-104.502	-107.479	-45.589	-51.005
C_{11} [GPa]	389	532	626	419	434
C_{12} [GPa]	119	122	187	59	120
C_{44} [GPa]	60	121	144	55	109
Bulk Modulus [GPa]	204	259	333	179	225
Shear Modulus [GPa]		150	171	90	126
Young's Modulus [GPa]	385	486	540	405	382
Poisson's ration		0.187	0.230	0.124	0.217

Effect of 4+ ion substitution

The substitution of 4+ ions in the urania matrix does not change the electrostatic contribution of the overall system. However, the elastic effect due to the ionic radii of the substituted

ions will guide the variation of lattice parameter and elastic properties of the urania matrix. The ionic radii of Ce^{4+}, U^{4+} and Th^{4+} are 0.97 Å, 1.00 Å and 1.05 Å respectively [13]. Therefore, Ce^{4+} ions are smaller and Th^{4+} ions are larger than the host U^{4+} ions.

Effect of Ce^{4+} ion substitution

Grimes and Nadeem potentials are used to estimate the effect of Ce^{4+} ion substitution. Following experimental characterization, the change in lattice parameter is evaluated for $U_{1-x}Ce_xO_2$ system where $x \leq 0.4$. The Ce^{4+} ions are randomly distributed in the urania matrix to represent solid solution. Multiple simulations are performed at each concentration to obtain an average lattice parameter. Considering the average values at each concentration, a maximum deviation of ±0.0005% is observed for 40% Ce^{4+} substitution. Since the deviation in lattice parameter is observed to be very insignificant, sophisticated methods like SQS approach is expected to have very minor effect on the predicted lattice parameters. Figure 1 illustrates the comparison of the absolute change in lattice parameter predicted by the two potentials with experiment. Even though the quantitative predictions of the UO_2 lattice parameter by Grimes and Nadeem differ from the experiment, the slopes of the change in lattice parameter with concentration of Ce^{4+} are comparable with experiment. Thus, using the atomistic models we have successfully calculated the variation in lattice parameter of Ce^{4+} ion substituted urania system. The results show that the elastic effect due to the substitution of a smaller ionic radius cation (Ce^{4+} = 0.97 Å compared to U^{4+} = 1.00 Å) reduces the overall lattice parameter of the system.

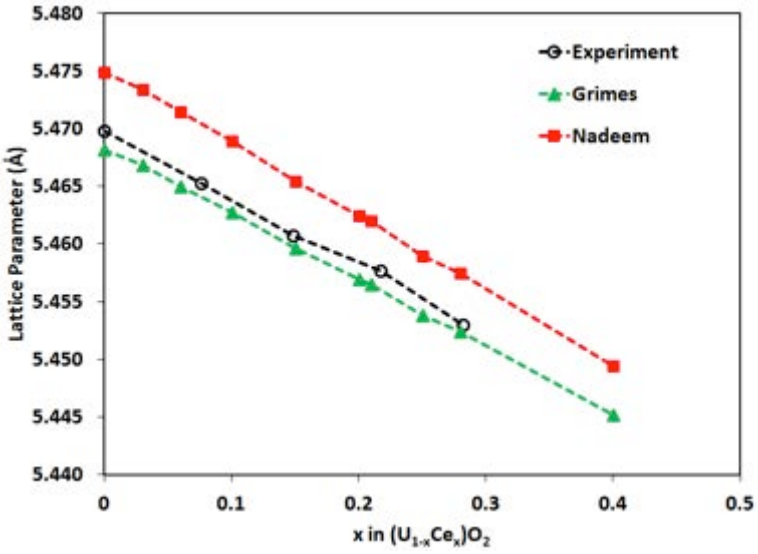

Figure 1. (Color online) Variation of lattice parameter due to 4+ ion substitution in $U_{1-x}Ce_xO_2$ system

Since the lattice parameter of the urania matrix changes due to substitution at a constant temperature and oxygen stoichiometry, it is possible to estimate the lattice variation with a physical parameter known as chemical expansion. Similar to thermal expansion, the chemical expansion measures the change in lattice parameter due to the change in chemical formula of the urania

matrix. While temperature is the guiding variable for thermal expansion, the substituted ionic species is the guiding factor for chemical expansion. For most of the materials the thermal expansion is positive, while chemical expansion can be either positive or negative depending on the ionic radii and charge state of the substituted ions. Therefore, the chemical expansion for the $U_{1-x}Ce_xO_2$ system can be defined as [14]

$$\varepsilon_C = \left.\frac{(a - a_0)}{a_0}\right|_{T=\text{Constant}} \quad (5)$$

where a is the lattice parameter measured at any concentration, and a_0 is the lattice parameter of UO_2 perfect lattice. During fission different concentration of fission products are produced in the fuel. This chemical expansion can be used to relate the effect of individual fission products on the overall structural and elastic properties of the fuel. In this study we have focused on the effect of Ce^{4+} and Th^{4+} ions. Table III lists the chemical expansion with Ce^{4+} ion concentration for the empirical models. For a single crystal, a variation in lattice parameter is the same as the variation in length. Thus, for all the compositions analyzed $(a - a_0) / a_0 = (L - L_0) / L_0$, where L is the length of the supercell measured with substituted ions, and L_0 is the length of the supercell for perfect UO_2.

Effectively, the reduction in lattice parameter of the urania matrix may be achieved by a change in temperature. The change in temperature (ΔT_{eq}) necessary to achieve the same amount of variation in pure UO_2 as observed for the substitution of different concentration of Ce^{4+} ions may be calculated as:

$$\varepsilon_C = \alpha_{T,bulk\,UO_2}\,\Delta T_{eq} \quad (6)$$

where, ε_c is the chemical expansion calculated from the simulations, and $\alpha_{T,bulkUO2}$ is the coefficient of thermal expansion reported for bulk UO_2 11.8 x 10^{-6} K^{-1} [15] from experiment. The ΔT_{eq} values estimated for different concentration of Ce^{4+} ions is reported in table III. For example, the ε_c observed for $U_{0.79}Ce_{0.21}O_2$ system is equivalent to reducing the temperature by ~181 - 200 K for bulk UO_2.

Table III. Chemical expansions calculated for Ce^{4+} ion substitution in $U_{1-x}Ce_xO_2$ system using Grimes and Nadeem potentials.

	x	a_0 (Å)	a (Å)	Δa (Å)	ε_C	ΔT_{eq} (K)
Grimes	0	5.4681				
	0.06		5.4650	-0.0031	-0.0006	-49
	0.15		5.4596	-0.0085	-0.0016	-132
	0.21		5.4565	-0.0117	-0.0021	-181
	0.28		5.4524	-0.0157	-0.0029	-244
Nadeem	0	5.4749				
	0.06		5.4714	-0.0035	-0.0006	-54
	0.15		5.4655	-0.0094	-0.0017	-146
	0.21		5.4620	-0.0129	-0.0024	-200
	0.28		5.4575	-0.0174	-0.0032	-270

Effect of Th^{4+} ion substitution

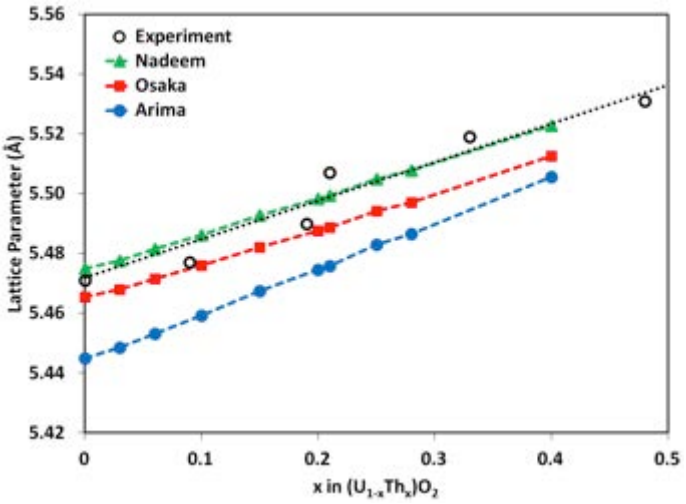

Figure 2. (Color online) Variation of lattice parameter due to 4+ ion substitution in $U_{1-x}Th_xO_2$ system. The open circles are experimental data with the dotted line indicating a linear fit.

Similar analysis is performed for Th^{4+} ion substitution in the UO_2 matrix with the variation in lattice parameter presented in figure 2. The experimental data points show a non-linear lattice expansion for the mixed $U_{1-x}Th_xO_2$ system. Here the lattice parameter of urania matrix increases with Th^{4+} ion substitution, contrary to Ce^{4+} ion substitution. This response is also due to the elastic effect. Th^{4+} ions are about 5% larger than the U^{4+} ions. Substitution of Th^{4+} ions creates local tension in the lattice, thereby increasing the overall lattice parameter. The ε_c, and ΔT_{eq} values for different potentials and compositions are calculated in the same manner as discussed for Ce^{4+} systems (using Eqs. 5 and 6).

Summary of Ce^{4+} and Th^{4+} ion substitution on lattice parameter

In order to directly compare ceria and thoria substitution, we took one nominal concentration (20%) of the dissolved ions in UO_2. Figure 3 shows the percentage change in lattice parameter predicted for $U_{1-x}A_xO_2$, where x=0.2, and A = Ce and Th. For 20% substitution, the lattice parameter decreases by ~0.22 ± 0.01 % for ceria and increases by ~0.46 ± 0.08 % for thoria. The results clearly indicate that the variation in lattice parameter for 4+ ion substitution is guided by the ionic radius (elastic effect) of the substituted ion.

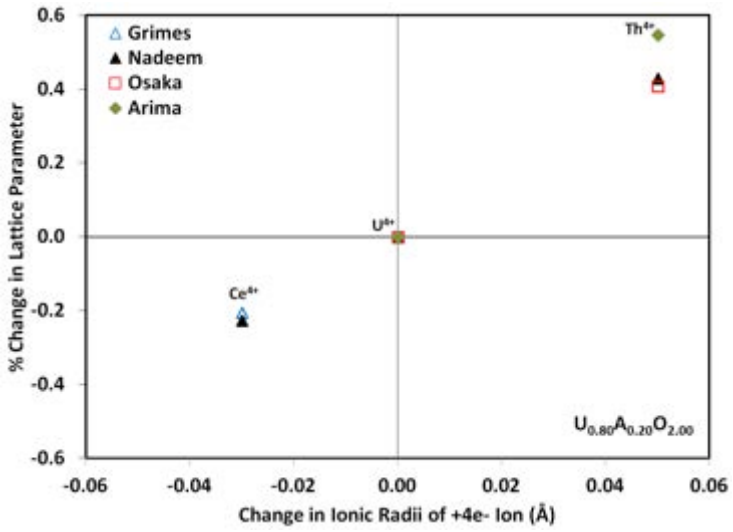

Figure 3. (Color online) Variation of lattice parameter due to Ce^{4+} and Th^{4+} ion substitution in $U_{1-x}A_xO_2$ system, where x = 0.20.

Effect of Ce^{4+} and Th^{4+} ion substitution on bulk modulus

The experimental bulk modulus of CeO_2 and ThO_2 are listed in table IV. We have used the experimental elastic constants (C_{11} and C_{12}) [16-18] to estimate the bulk modulus of UO_2, CeO_2 and ThO_2, where the bulk modulus is given as $(C_{11} + 2C_{12}) / 3$. This approach allows us to directly compare the single crystal bulk modulus values predicted from the simulations with experimental bulk modulus. The analysis of experimental bulk modulus values show that there is almost no variation in bulk modulus between pure UO_2 and CeO_2 and the bulk modulus reduces for bulk ThO_2 compared to UO_2. The predicted bulk modulus values of pure UO_2, CeO_2, and ThO_2 with empirical potentials follow the experimental trend (table IV). However, Osaka potential predicted a higher bulk modulus for ThO_2 compared to UO_2, which is not surprising since it severely underestimated (~50%) C_{12} elastic constant for bulk UO_2 (table II). Using Vegard's law for the substituted systems, we should expect almost no variation for $U_{1-x}Ce_xO_2$ system and a reduction in bulk modulus for $U_{1-x}Th_xO_2$ system.

Table IV. Bulk modulus values calculated for UO_2, CeO_2 and ThO_2 by all the interatomic potentials. The results are compared to experimental results.

in GPa	UO_2	CeO_2	ThO_2
Experiment*	209-212 [17]	204 [16]	193 [18]
Grimes	259	268	

Nadeem	333	333	303
Osaka	179		206
Arima	225		192

*Calculated using elastic constants reported in the experiment

Since Nadeem is the only potential which described both Ce^{4+} and Th^{4+} ions, the variation in bulk modulus with concentration is discussed for this potential. Figure 4 shows the effect of substitution on the bulk modulus for $U_{1-x}Ce_xO_2$ and $U_{1-x}Th_xO_2$ system using Nadeem potential. The results clearly show almost no effect on the bulk modulus for $U_{1-x}Ce_xO_2$ and a gradual reduction for $U_{1-x}Th_xO_2$ system. This is in agreement with the Vegard's law prediction from the experimental bulk modulus reported in table IV.

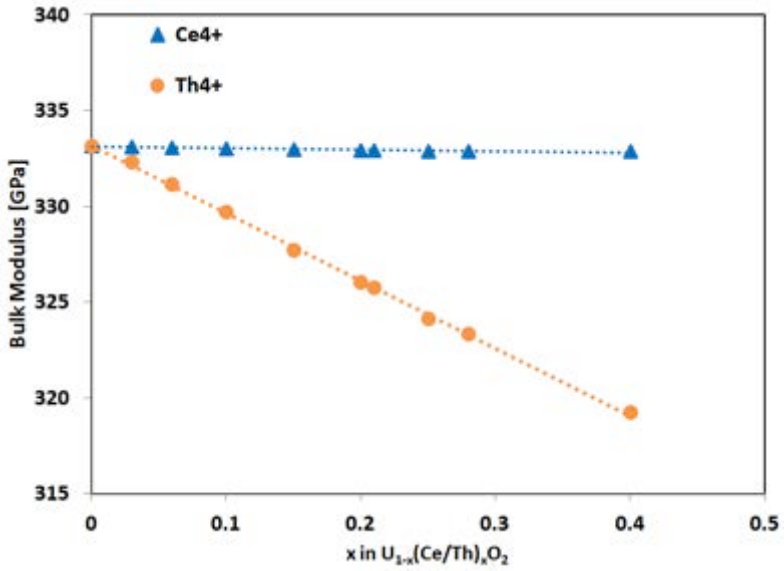

Figure 4. (Color online) Variation of bulk modulus for a range of Ce^{4+} and Th^{4+} ion substitution in urania matrix using Nadeem potential. Substitution of Ce^{4+} shows very minimal variation in bulk modulus, while the modulus decreases with Th^{4+} ion substitution in urania.

CONCLUSIONS

This study presented the effect of substitution on the structural and elastic properties of $U_{1-x}A_xO_2$ system (A = Ce and Th). Using atomistic simulations with empirical potentials we have

presented that the overall lattice parameter variation is guided only by the elastic effect for 4+ ion substitution in UO_2. The lattice parameter decreases for a smaller ionic radii and increases for a larger ionic radii substitution in the urania matrix. The variation in lattice parameter due to substitution is used to estimate the equivalent temperature change necessary to achieve similar lattice response for pure UO_2. In particular, our simulation results show that the chemical expansion observed for $U_{0.79}Ce_{0.21}O_2$ system is equivalent to reducing the temperature by ~181 - 200 K for bulk UO_2. Similarly, the chemical expansion observed for $U_{0.79}Th_{0.21}O_2$ system is equivalent to increasing the temperature by ~360 - 482 K for bulk UO_2. The analysis of bulk modulus shows that the elastic property is well maintained for the $U_{1-x}Ce_xO_2$ system, however, the bulk modulus values decreases for the $U_{1-x}Th_xO_2$ system.

Overall, atomic level simulation is a powerful tool to estimate the structural and elastic properties of $U_{1-x}A_xO_2$ system. It is necessary to estimate the effect of 3+ ion substitution in the urania matrix. The effect of 3+ ion substitution is expected to be more complex due to both elastic and electrostatic effects. In order to maintain charge neutrality, oxygen vacancies have to be introduced into the system. A systematic study of 4+ and 3+ ion substitutions in the urania matrix will be very important to address the physical and chemical properties of FPs and MAs on the nuclear fuel. In addition fixed charge models, like the one used in this study, do not allow the change in charge due to substitution. Therefore, more sophisticated methods like charge transfer potentials will be effective in investigating the local arrangement of substituted ions. However, it is necessary to point out that variable charge models are extremely difficult to develop for such systems.

ACKNOWLEDGEMENTS

This work was funded by DOE-NEUP DE-AC07-05ID14517 and NRC Faculty Development Grant. The authors want to thank Dr. H. Xu for valuable discussions on the structure of 4+ ion substitution.

Appendices A

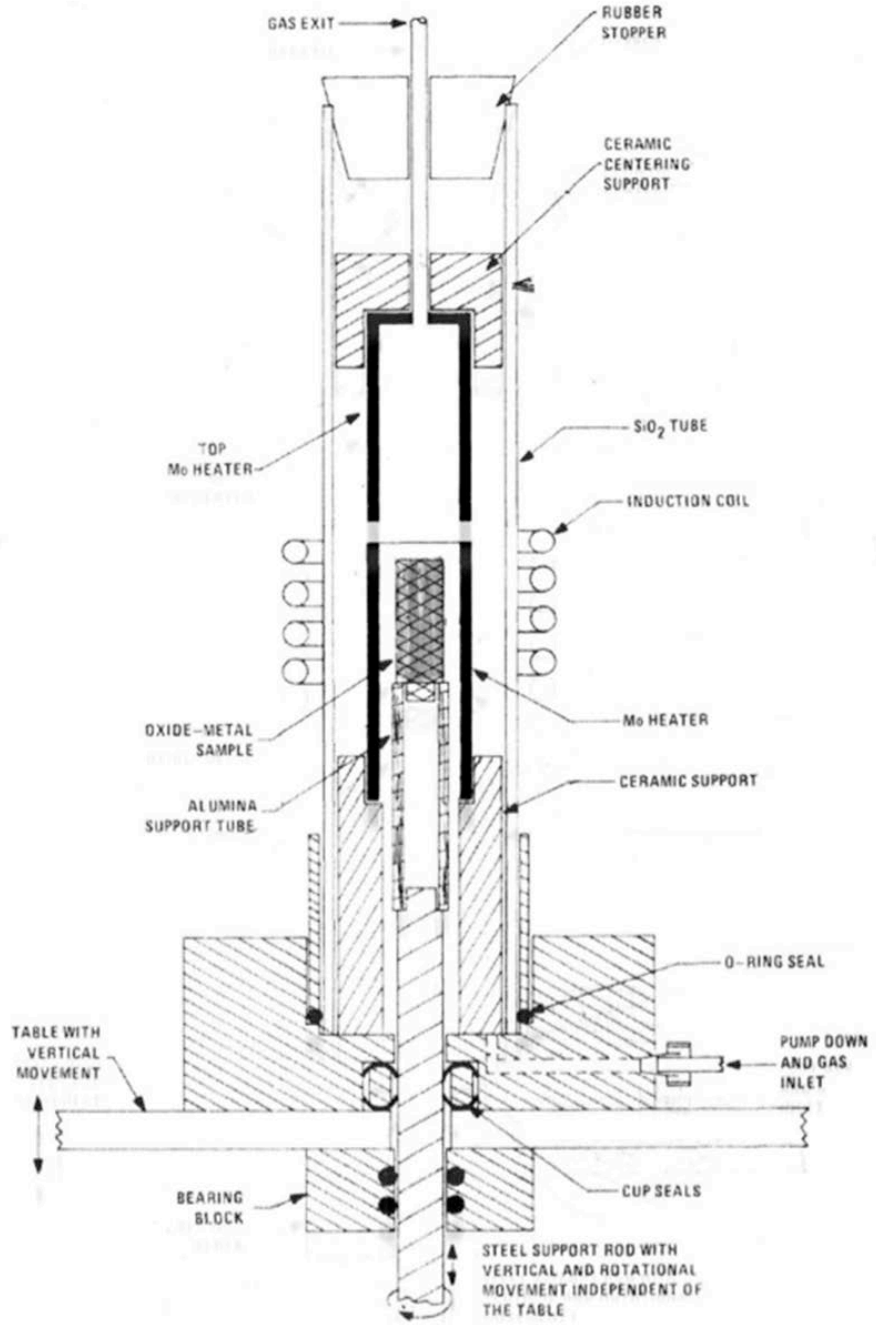

FIGURE 51 - CONCEPTUAL SCHEMATIC OF BULK SINGLE CRYSTAL GROWTH FURNACE

FIGURE 52 - HIGH FREQUENCY INDUCTION FURNACE (1-INCH INDUCTION COIL)

FIGURE 53 - POWER SUPPLY FOR INDUCTION FURNACE

FIGURE 54 - MATCHING NETWORK FOR INDUCTION FURNACE

FIGURE 55 - TEMPERATURE READ-OUT FOR INDUCTION FURNACE COOLING SYSTEM

FIGURE 56 - PYROMETER FOR READING OXIDE'S SKIN TEMPERATURE

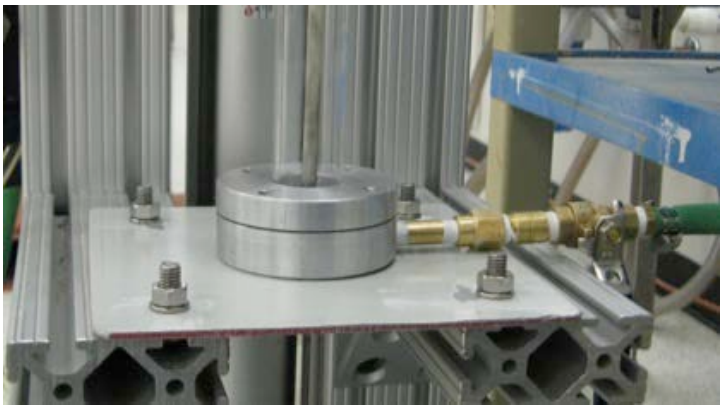

FIGURE 57 - BOTTOM ALUMINUM END CAP FOR FURNACE CHAMBER (1-INCH SET-UP)

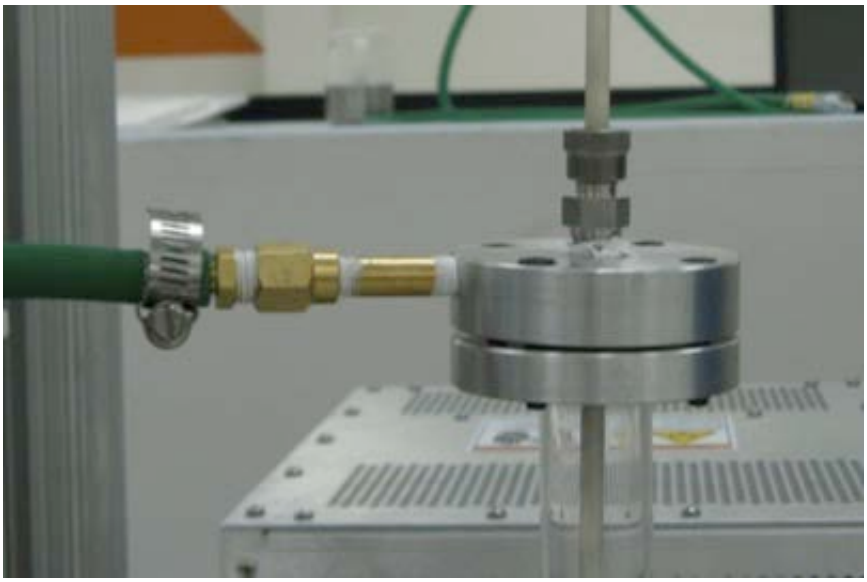

FIGURE 58 - UPPER ALUMINUM END CAP FOR FURNACE CHAMBER (1-INCH SET-UP)

FIGURE 59 - HYDRAULIC RAMP FOR LIFTING OXIDE SAMPLE

FIGURE 60 - EXHAUST SYSTEM FOR FURNACE CHAMBER

FIGURE 61 - COOLING SYSTEM FOR INDUCTION FURNACE

FIGURE 62 - GAS MANIFOLD SYSTEM FOR FURNACE CHAMBER

FIGURE 63 - GAS CYLINDER STAND FOR MULTIPLE GASES FOR CRYSTAL GROWTH PROCESS

FIGURE 64 - PERSONAL PROTECTION EQUIPMENT FOR CRYSTAL GROWTH PROCESS

FIGURE 65 - STEEL DIE SET FOR PRESSING OXIDE PELLET

FIGURE 66 - SPECIALLY DESIGN SINTERING PRESS

FIGURE 67 - PROCESS FOR PRESSING AN OXIDE PELLET

FIGURE 68 - PRESSED CERIUM (IV) OXIDE PELLET (MASS = 30 GRAMS)

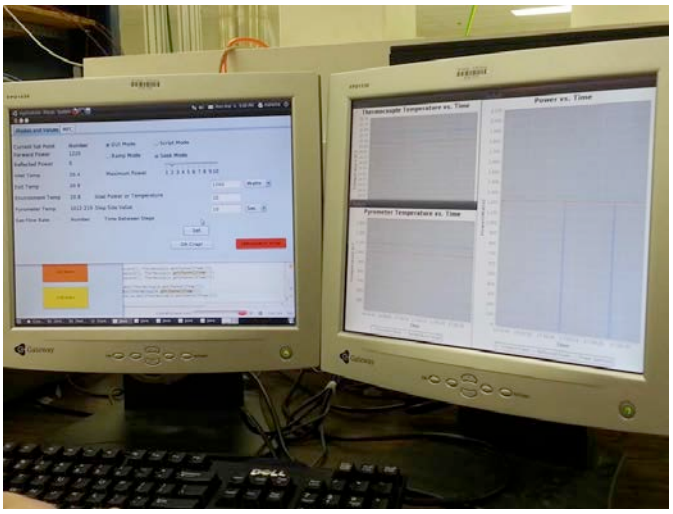

FIGURE 69 - COMPUTER INTERFACE FOR CONTROLLING INDUCTION FURNACE

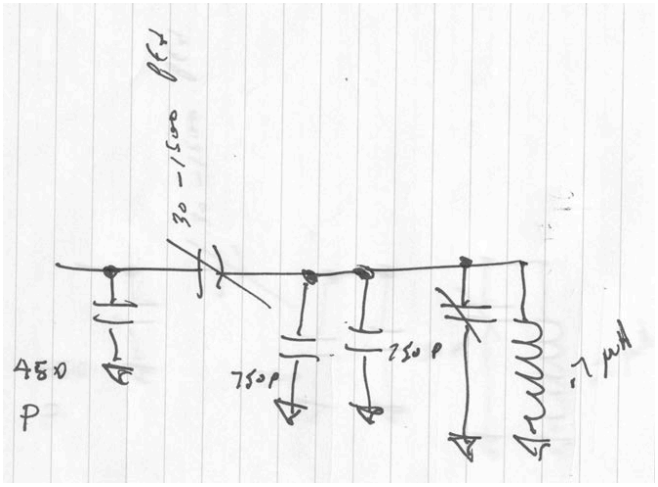

FIGURE 70 - ORIGINAL CIRCUIT FOR THE MATCHING NETWORK

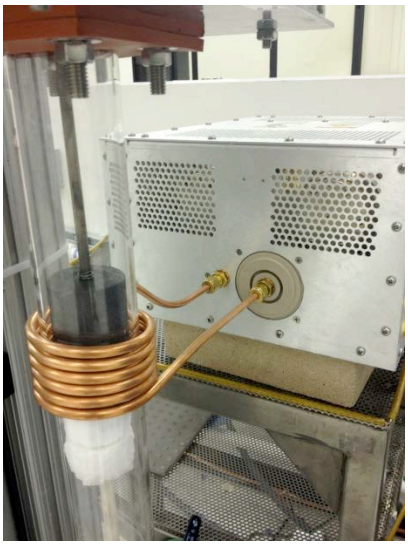

FIGURE 71 - 2-INCH INDUCTION COIL SETUP FOR FURNACE CHAMBER

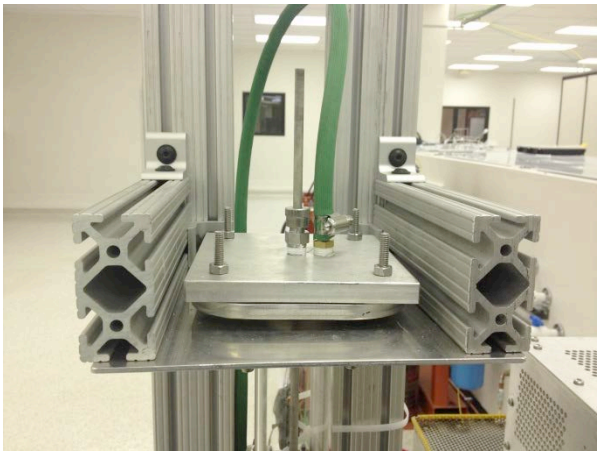

FIGURE 72 - UPPER ALUMINUM END CAP FOR FURNACE CHAMBER (2-INCH SET-UP)

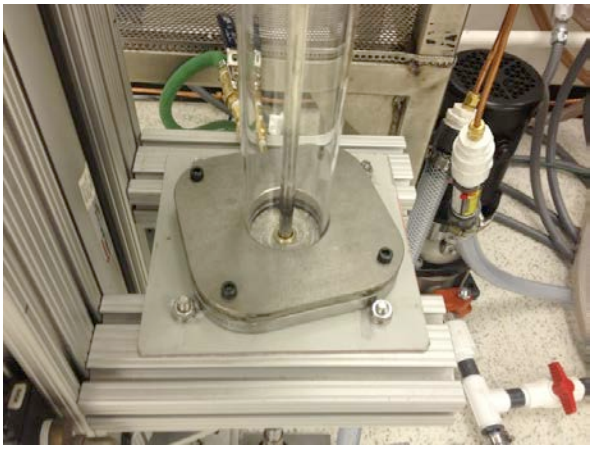

FIGURE 73 - BOTTOM STAINLESS STEEL END CAP FOR FURNACE CHAMBER (2-INCH SET-UP)

FIGURE 74 - NEW SET OF STEEL DIES FOR PRESSING OXIDE PELLET (1.5 –INCH ID LEFT, 1.75-INCH ID RIGHT)

FIGURE 75 - VERY HIGH TEMPERATURE CERAMIC PLATFORM FOR CRYSTAL GROWTH

FIGURE 76 - BACK RIGHT CORNER VIEW OF THE GLOVEBOX

FIGURE 77 - FRONT (RIGHT) AND BACK (LEFT) DOOR OF THE GLOVEBOX ANTECHAMBER

FIGURE 78 - FEEDTHROUGHS FOR THE GLOVEBOX CONNECTIONS

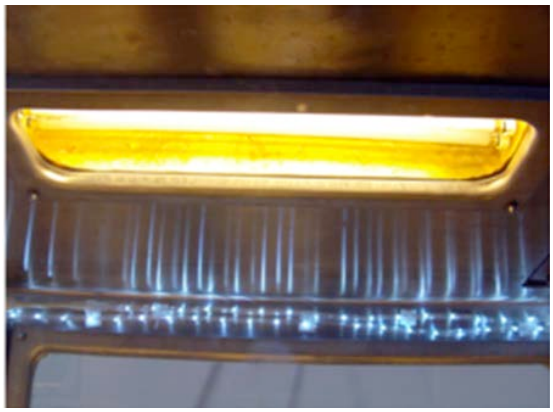

FIGURE 79 - INTERNAL AND EXTERNAL EMERGENCY LIGHTING SYSTEM

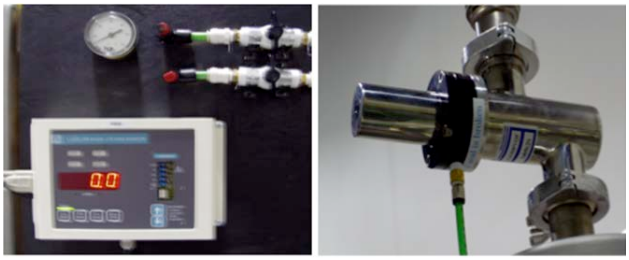

FIGURE 80 - ALARM SYSTEM CONSISTING OF ALPHA PARTICLE ISOLATION VALVE (RIGHT) AND DIGITAL READER (LEFT)

FIGURE 81 - ALARM SYSTEM CONSISTING OF SMOKE & HEAT DETECTORS (TOP), AND ALARMING PANELS (BOTTOM)

FIGURE 82 - VACUUM SYSTEM FOR THE PLUMBING OF THE GLOVEBOX

FIGURE 83 - MANOMETER FOR INTERNAL READOUT OF THE GLOVEBOX PRESSURE

FIGURE 84 - FILTRATION SYSTEM CONSISTING OF DRUM HEPA FILET (LEFT), SECONDARY FILTERED DIAPHRAGM VACUUM PUMP (MIDDLE), & SMALL ONE-WAY HEPA FILTER (RIGHT)

FIGURE 85 - INERT GAS SYSTEM FOR THE INDUCTION FURNACE (NITROGEN & OXYGEN)

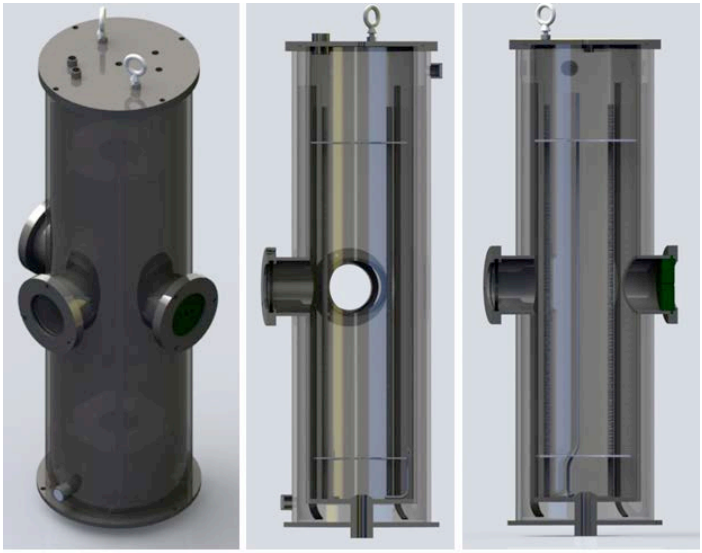

FIGURE 86 - SOLIDWORKS DESIGN OF THE RADIOACTIVE MATERIALS INDUCTION FURNACE

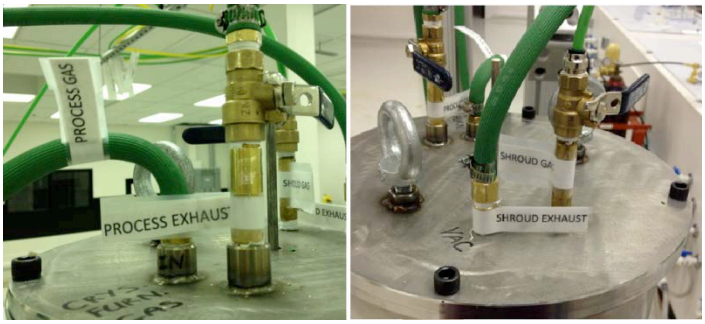

FIGURE 87 - SHROUD AND PROCESS GAS SYSTEM FOR RADIOACTIVE MATERIALS FURNACE

FIGURE 88 - VACUUM PUMP FOR PROCESS GAS SYSTEM

FIGURE 89 - UPDATED EXHAUST SYSTEM FOR RADIOACTIVE MATERIALS FURNACE

FIGURE 90 - INDUCTION COIL INSULATED FOR RADIOACTIVE MATERIALS FURNACE

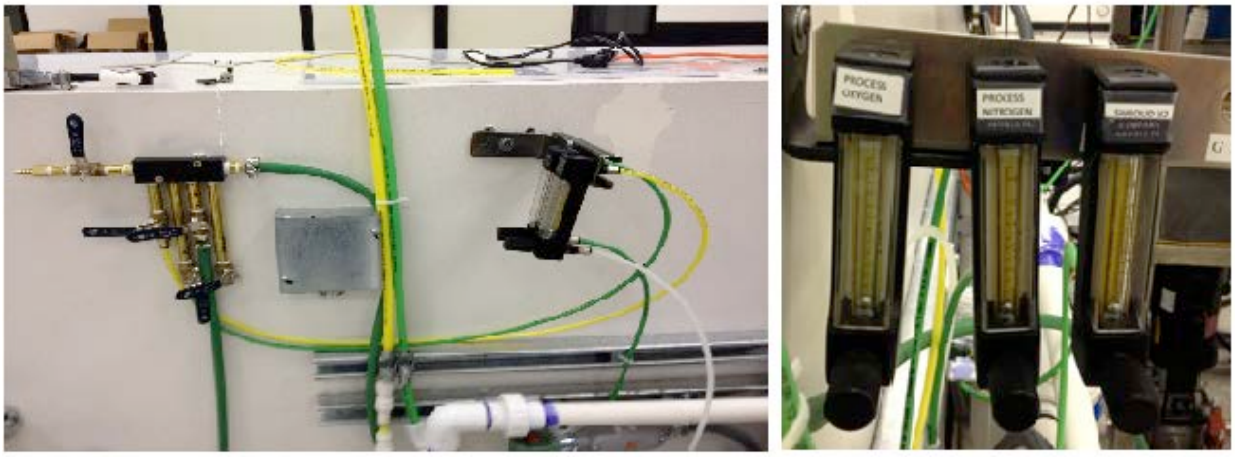

FIGURE 91 - UPDATED GAS MANIFOLD SYSTEM FOR RADIOACTIVE MATERIALS FURNACE

FIGURE 92 - COOLING SYSTEM FOR WATER JACKET INSIDE RADIOACTIVE MATERIALS FURNACE

FIGURE 93 - HEPA FILTER ON THE VACUUM PUMP FOR RADIOACTIVE MATERIALS FURNACE

FIGURE 94 - UPDATED STAINLESS STEEL HOSE FOR PROCESS GAS OUT

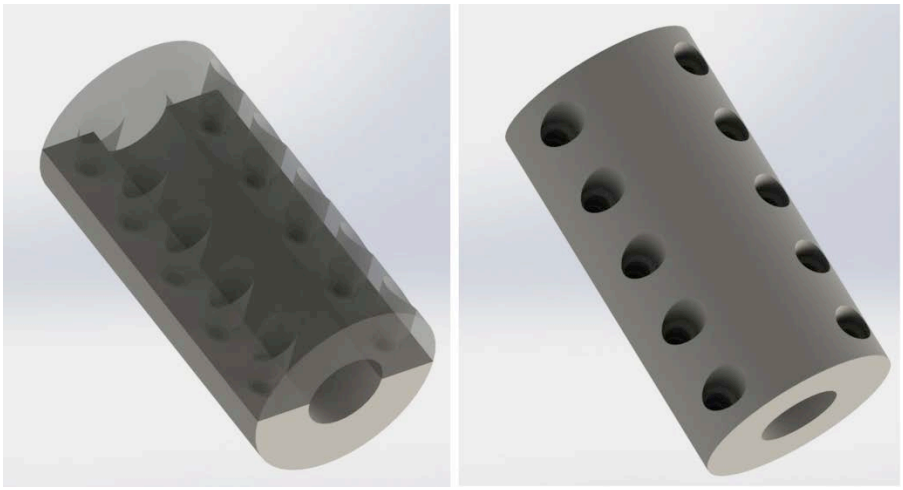

FIGURE 95 - SOLIDWORKS DESIGN OF NEW STEEL DIE FOR UO_2 MATERIAL

FIGURE 96 - STEEL DIE WITH MULTIPLE RODS FOR UO_2 POWDER (CROSS SECTIONAL VIEW)

FIGURE 97 - GRAPHITE SLEEVE & PUCKS FOR UO_2 PELLET PRESSING PROCESS

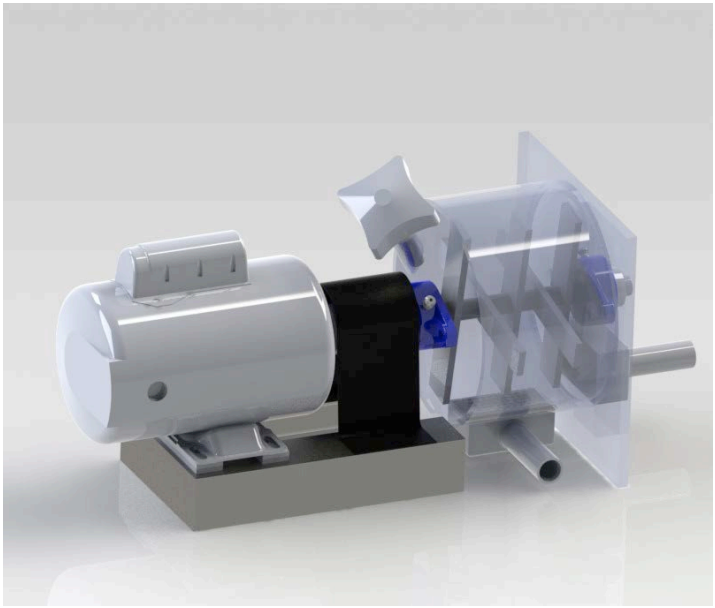

FIGURE 98 - SOLIDWORKS DESIGN OF THE HAMMER-MILL FOR CRUSHING UO_2 FUEL PELLETS

FIGURE 99 - HAMMER-MILL FOR CRUSHING UO_2 FUEL PELLETS

FIGURE 100 - 1200 °C TUBE FURNACE FOR ANNEALING & SINTERING OXIDE PELLETS

FIGURE 101 - 1600 °C TUBE FURNACE FOR ANNEALING & SINTERING OXIDE PELLETS

FIGURE 102 - 1.5-INCH OD SINTERED UO_2 PELLETS

FIGURE 103 - 70 KW INDUCTION FURNACE DURING GRAPHITE TESTING

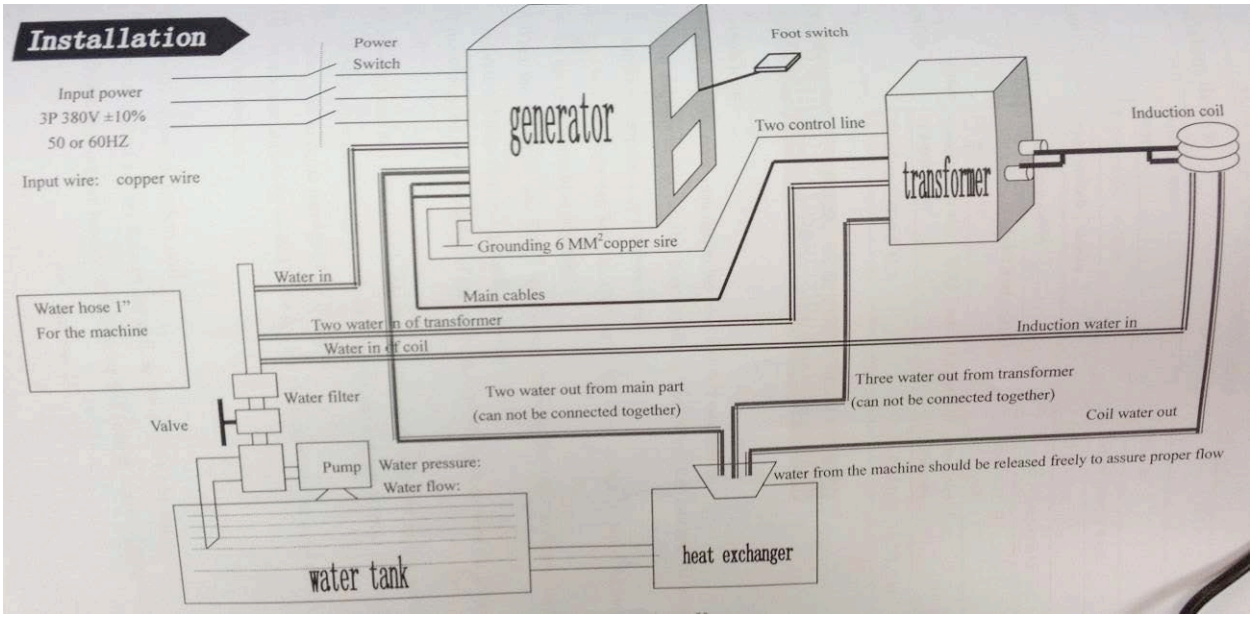

FIGURE 104 - INSTALLATION MANUAL FOR 70 KW SINTERING INDUCTION FURNACE

FIGURE 105 - STEPPER LIFT & ROTATE MOTORS FOR CRYSTAL GROWTH

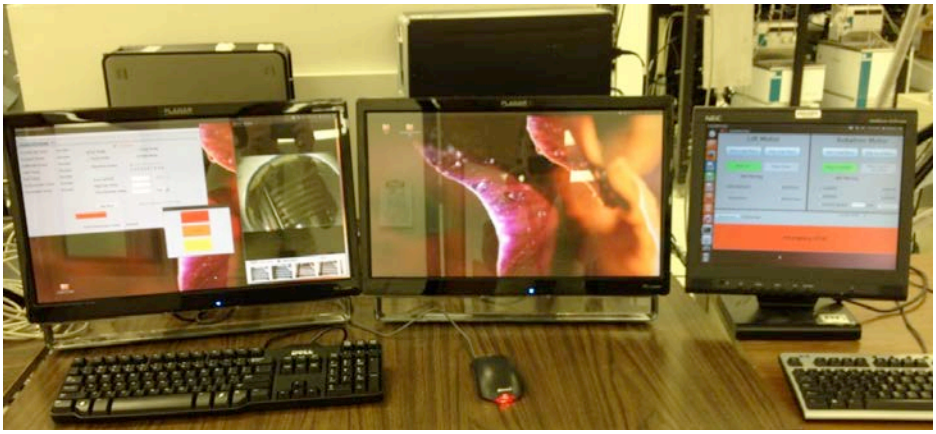

FIGURE 106 - COMPUTER INTERFACE FOR INDUCTION FURNACE & STEPPER MOTORS

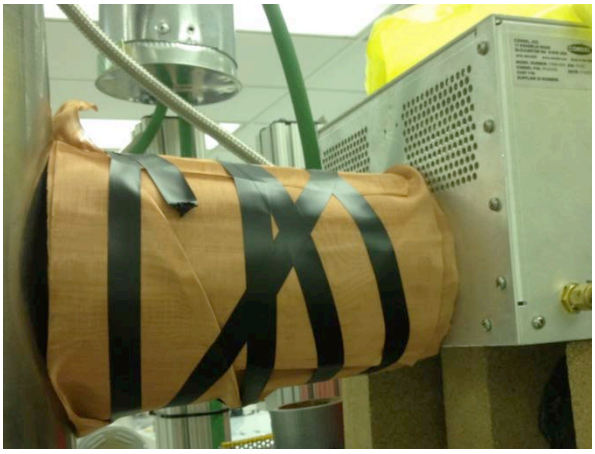

FIGURE 107 - INDUCTION RF BLOCKAGE WITH POLYCARBONATE (PC) TUBE & COPPER MESH

Appendices B

FIGURE 108 - CeO_2 RAW CRYSTAL (BEFORE ANNEALING) SAMPLE FROM 01-31-13 RUN, VIEW 1 (CHEAPER STOCK MATERIAL)

FIGURE 109 - CeO_2 RAW (BEFORE ANNEALING) CRYSTAL SAMPLE FROM 01-31-13 RUN, VIEW 2 (CHEAPER STOCK MATERIAL)

FIGURE 110 - CeO_2 RAW (BEFORE ANNEALING) CRYSTAL SAMPLE FROM 01-31-13 RUN, VIEW 3 (CHEAPER STOCK MATERIAL)

FIGURE 111 - CeO_2 DURING CRYSTAL GROWTH (MOLTEN PHASE)

FIGURE 112 - FIRST GROWTH OF CeO_2 FROM 01-25-13 RUN (CRACKED FROM CRUCIBLE), QUARTER PLACED NEXT FOR SIZE REFERENCE

FIGURE 113 - SEPARATED CeO_2 SINGLE CRYSTAL FROM 03-04-13 RUN (AFTER ANNEALING AND PRIOR TO CUTTING & POLISHING)

FIGURE 114 - LARGE CeO_2 BI-CRYSTAL FROM 03-03-13 RUN (AFTER ANNEALING AND PRIOR TO CUTTING & POLISHING)

FIGURE 115 - LARGE (~2 CM) CeO_2 SINGLE CRYSTAL FROM 03-03-13 RUN (AFTER ANNEALING AND PRIOR TO CUTTING & POLISHING)

FIGURE 116 - TOP VIEW OF 1 MM THIN CUT OF CeO_2 CRYSTAL FROM 03-04-13 RUN

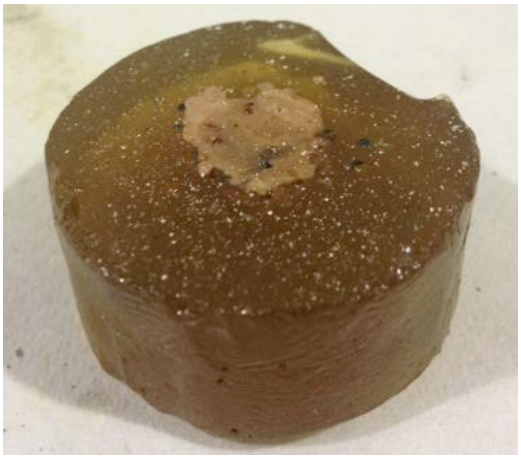

FIGURE 117 - CEO_2 CRYSTAL CUT & POLISHED FROM 03-04-13 RUN (STILL IN WAX CASTING)

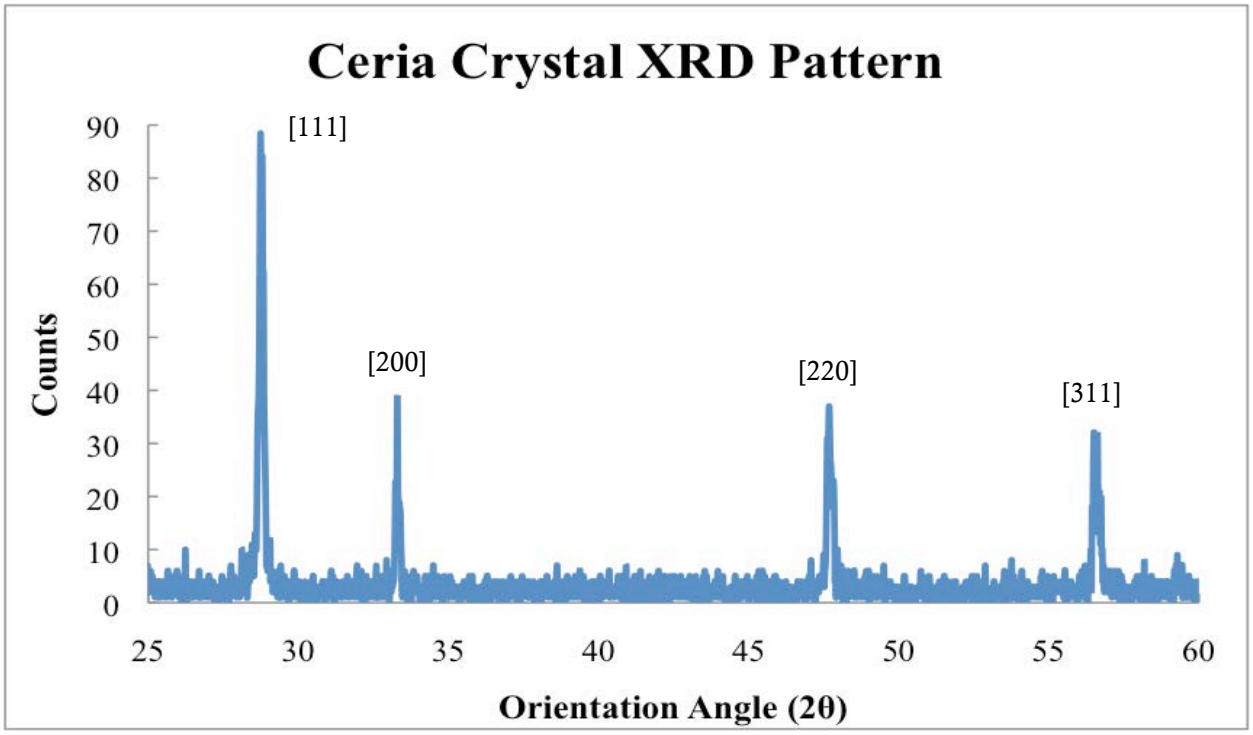

FIGURE 118 - XRD SPECTRUM FOR CeO_2 CRYSTAL CUT & POLISHED FROM 03-04-13 RUN

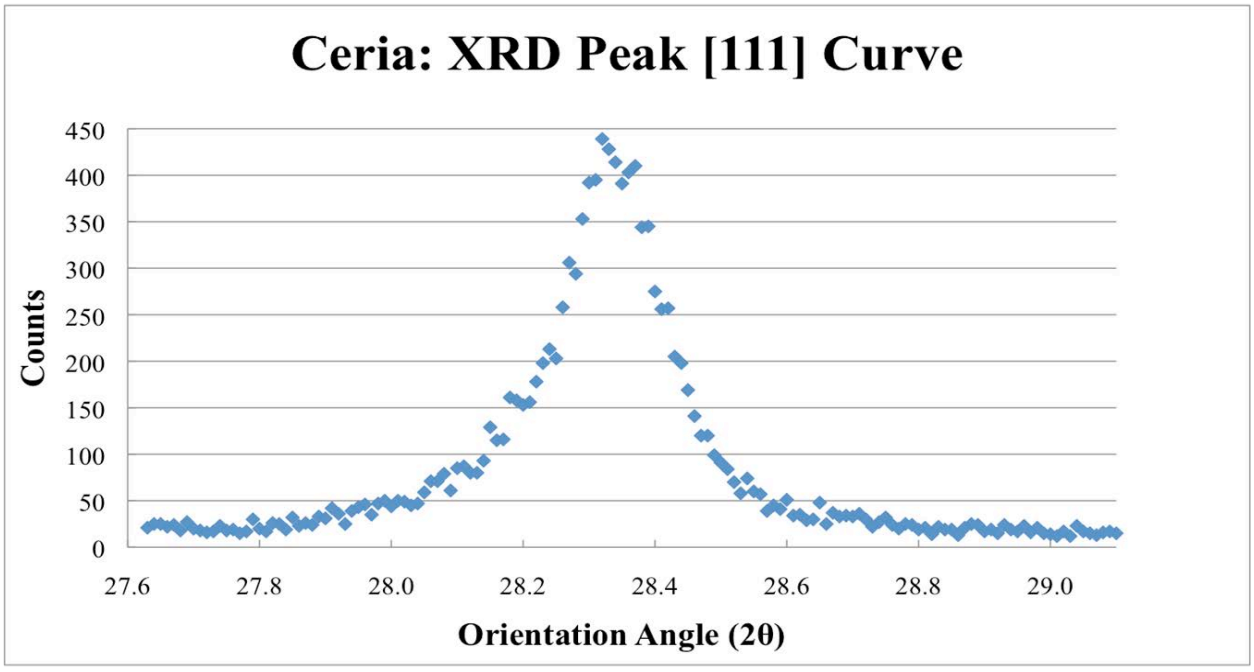

FIGURE 119 - XRD RESULTS ON CERIA PEAK [111] (FWHM = 297 ARCSEC)

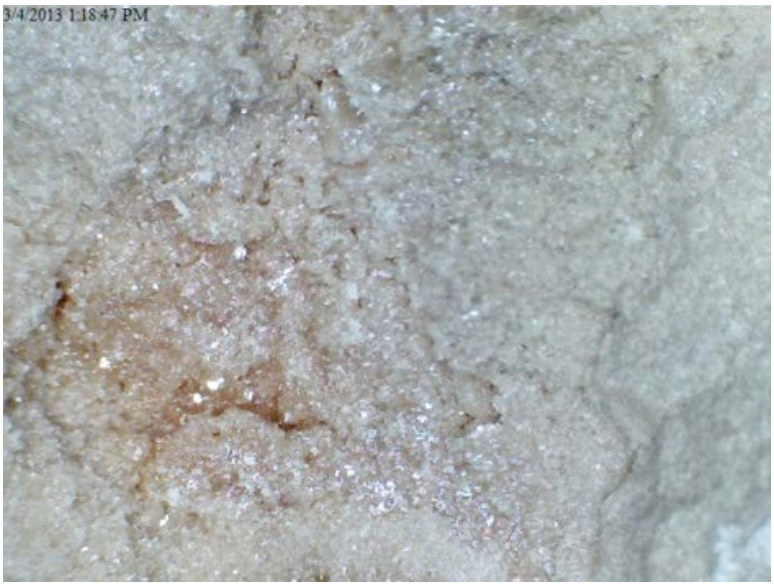

FIGURE 120 - RAW CERIA CRYSTAL FROM 03-07-13 RUN AFTER ANNEALING

FIGURE 121 - RAW CERIA CRYSTAL FROM 03-11-13 RUN AFTER ANNEALING

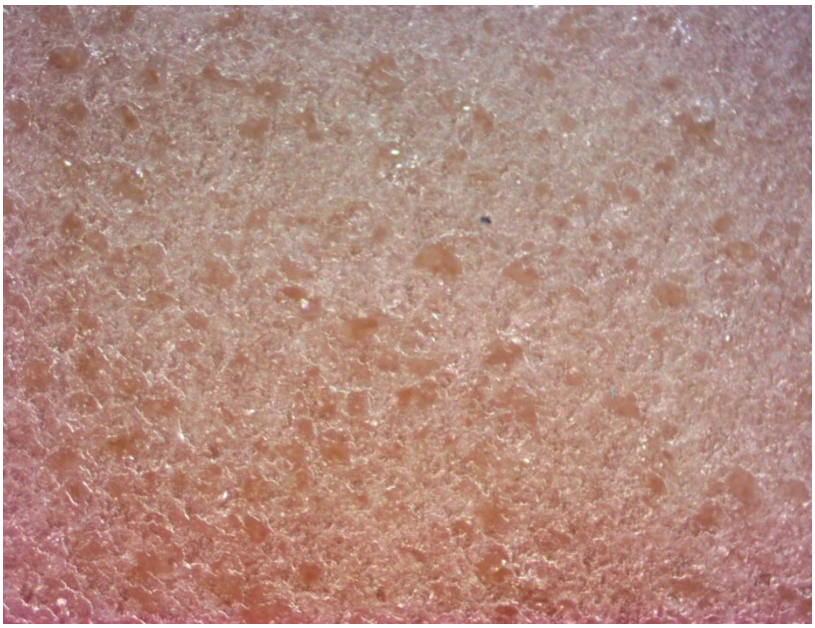

FIGURE 122 - CUT & POLISHED CERIA CRYSTAL FROM 03-11-13 RUN, VIEW 1

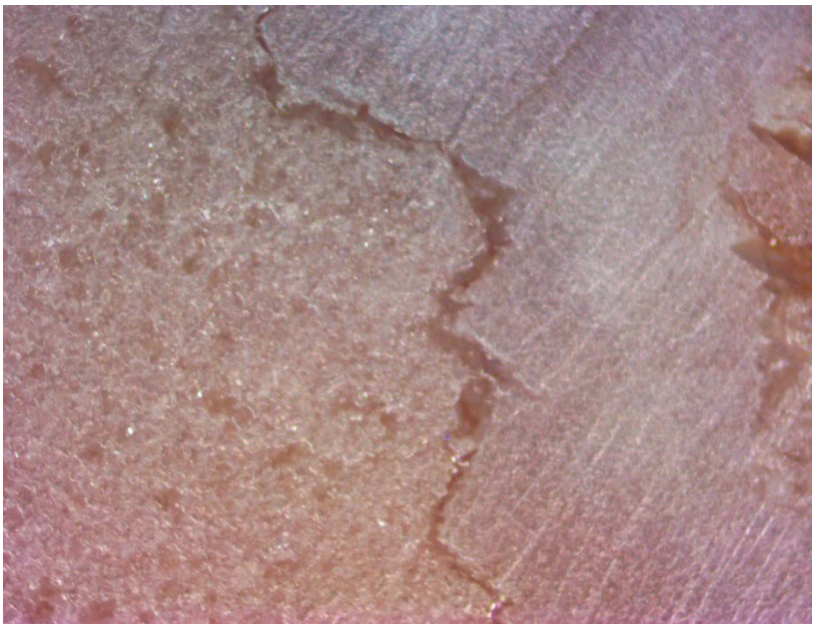

FIGURE 123 - CUT & POLISHED CERIA CRYSTAL FROM 03-11-13 RUN, VIEW 2

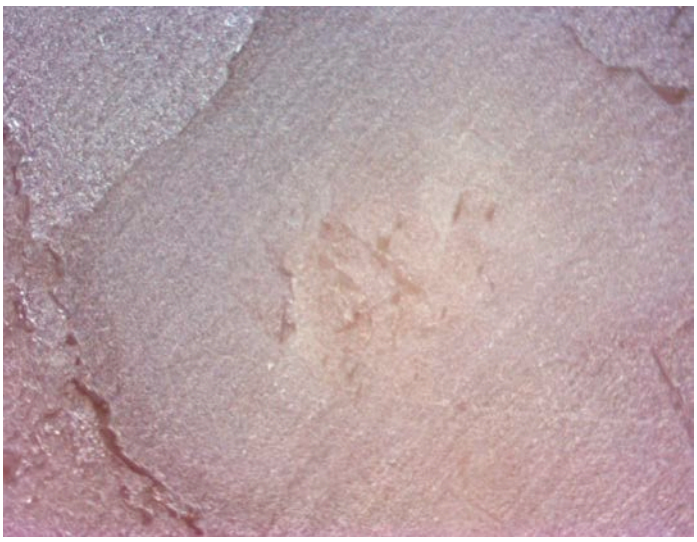

FIGURE 124 - CUT & POLISHED CERIA CRYSTAL FROM 03-11-13 RUN, VIEW 3

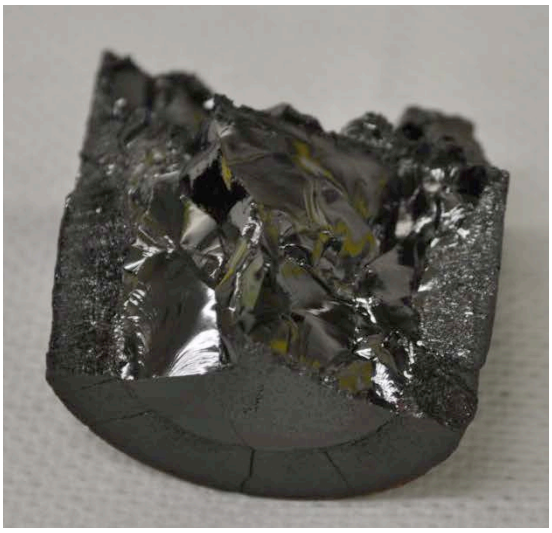

FIGURE 125 – UO_2 RAW CRYSTAL BEFORE CUT OR POLISH, VIEW 1

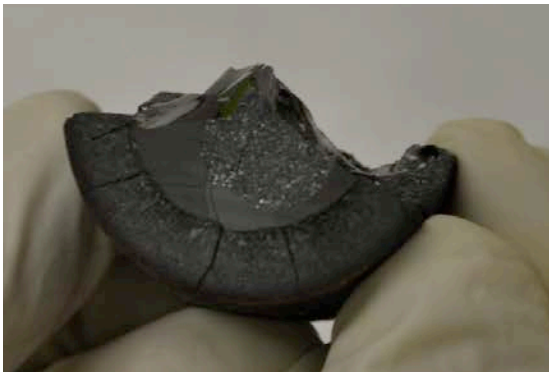

FIGURE 126 - UO_2 RAW CRYSTAL BEFORE CUT OR POLISH, VIEW 2

FIGURE 127 – LARGE SINGLE CRYSTAL OF UO_2 BEFORE CUT OR POLISH

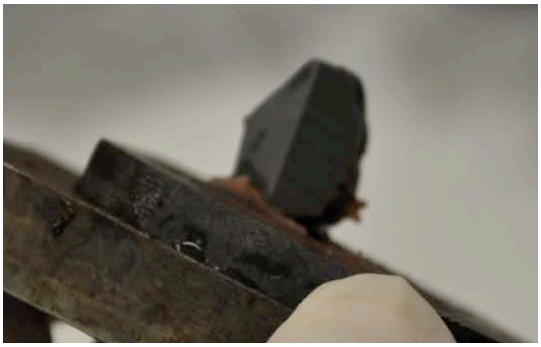

FIGURE 128 – SMALL PIECE OF UO_2 CRYSTAL BEING CUT

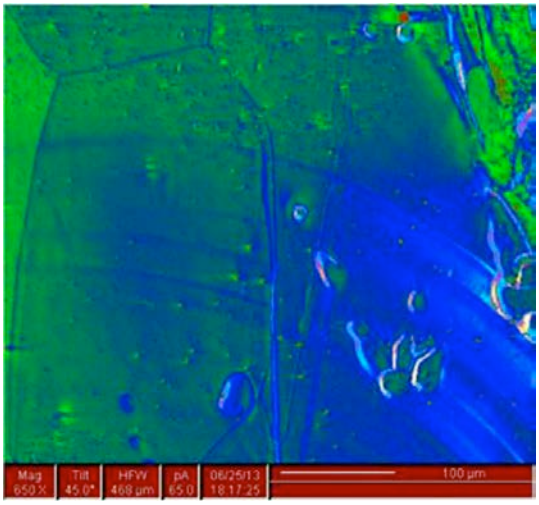

FIGURE 129 – FIB IMAGE OF A SMALL PIECE OF RAW UO_2 CRYSTAL (UNCUT OR UNPOLISHED)

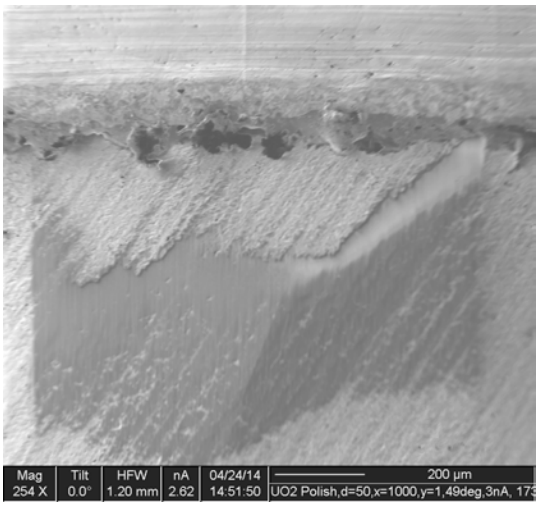

FIGURE 130 – FIB IMAGE OF CUT AND POLISHED PIECE OF UO_2 CRYSTAL (TRI-CRYSTAL INTERFACE), VIEW 1

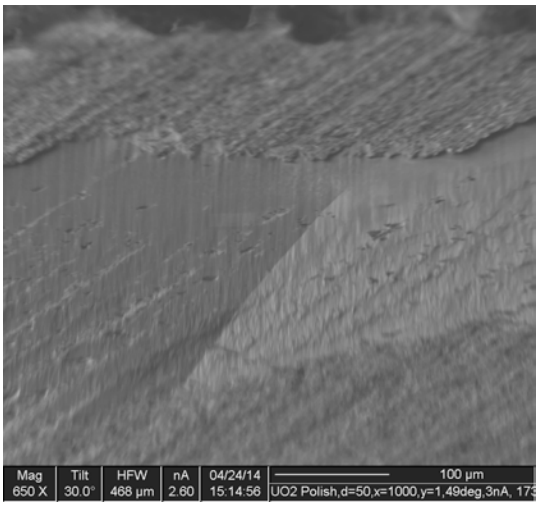

FIGURE 131 - FIB IMAGE OF CUT AND POLISHED PIECE OF UO_2 CRYSTAL (TRI-CRYSTAL INTERFACE), TILTED VIEW 2

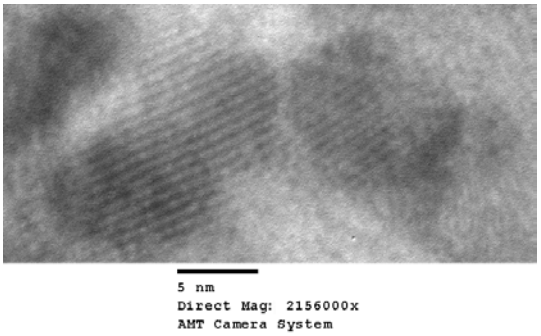

FIGURE 132 – TEM IMAGE OF UO_2 CRYSTAL IDENTIFYING INTERFERENCE PATTERN

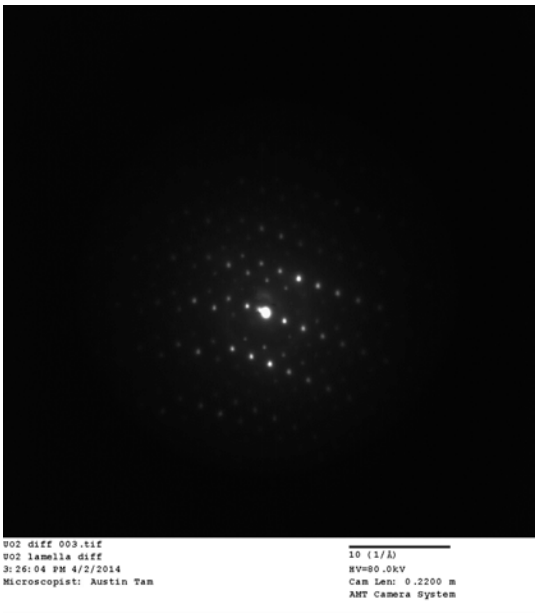

FIGURE 133 – DIFFRACTION PATTERN OF UO_2 CRYSTAL ON TEM GRID

Patents/Publications/Presentations

Milestones

Milestone Description	Planned Completion Date	Percent Complete	Type	Major Milestone Comments
Install and Commission new crystal furnace and obtain required RAM licensing	12/1/2011	100%	Major	Complete.
Grow, process (Cut/polish), and characterize the first single crystal bulk sample	7/1/2012	100%	Major	Complete
Grow first layers of fission product surrogates on urania crystals	4/1/2012	100%	Minor	Complete
Grow and characterize the first MOCVD grown engineered crystal sample	10/12/2012	100%	Major	Complete
Commission new fuel furnace	12/1/2011	100%	Minor	Complete
Results from first round of irradiation tests will be collected	1/1/2013	100%	Major	Complete
First models will be run simulating the first experiments	4/1/2013	100%	Major	Complete.

Students

Students currently funded to date at ISU are:

Amanda Finkes, Brycen Wendt, Berkley Starks, Jenna Deaven, Verena Kleinrath, Derick Tromblin, Holly Thornton, Samuel Haroldson, and Malwina Chaczko.

Budget Data

Project Complete.

References:

[1] Hirth J P and Lothe J 1982 *Theory of Dislocations* (New York: Wiley)

[2] Bulatov V V and Wei Cai 2006 *Computer simulations of dislocations* (Oxford University press)

[3] Olander D. R. 1976 Fundamental Aspects of Nuclear Reactor Fuel Elements, TID-26711-P1, National Technical Information Services

[4] Hull D and Bacon D J 1984 Introduction to Dislocations, Internation Series on Materials Science and Technology (Oxford: Pergamon)

[5] 1. C. B. Basak, A. K. Sengupta, and H. S. Kamath, J. Alloys Compd. 360 (2003) 210.

[6] M. P. Allen and D. J. Tildesley, *Computer Simulations of Liquids* (Oxford University Press, Oxford, 1987).

[7] G. Busker, R. W. Grimes, M. R. Bradford, J. Nucl. Mater. 312 (2003) 156-162

[8] D. C. Parfitt, C. L. Bishop, M. R. Wenman and R. W. Grimes, J Phys-Condens Mat 22,175004

[9] P. Nerikar, C. R. Stanek, S. R. Phillpot, S. B. Sinnott and B. P. Uberuaga, Phys. Rev. B, 81, (2010).

[10] Kleykamp, H. 1985 J. Nucl. Mater. 131, 221

[11] P.T. Sawbridge and E. C. Sykes, J. Nucl. Mater. 35 (1970) 122-125

1. H. Kleykamp, *J. Nucl. Mater.* **131**, 221-246 (1985).
2. K. Govers, S. Lemehov, M. Hou, and M. Verwerft, *J. Nucl. Mater.* **366**, 161-177 (2007).
3. R. W. Grimes and G. Busker, *Nucl. Energ.-J. Br. Nucl.* **35**, 403-410 (1996).
4. M. Nadeem, M. J. Akhtar, R. Shaheen, M. N. Haque, and A. Y. Khan, *J. Mater. Sci. Technol.* **17**, 638-642 (2001).
5. T. Arima, S. Yamasaki, Y. Inagaki, and K. Idemitsu, *J. Alloys Compd.* **400**, 43-50 (2005).
6. M. Osaka, J. Adachi, K. Kurosaki, M. Uno, and S. Yamanaka, *J. Nucl. Sci. Technol.* **44**, 1543-1549 (2007).
7. R. A. Buckingham, *Proc. R. Soc. London, Ser. A* **168**, 264-283 (1938).

8. P. M. Morse, *Phys. Rev.* **34**, 57-64 (1929).

9. B. G. Dick and A. W. Overhauser, *Phys. Rev.* **112**, 90-103 (1958).

10. J. D. Gale, *J. Chem. Soc., Faraday Trans.* **93**, 629-637 (1997).

11. J. D. Gale and A. L. Rohl, *Mol. Simulat.* **29**, 291-341 (2003).

12. D. J. Kim, Y. W. Lee, and Y. S. Kim, *J. Nucl. Mater.* **342**, 192-196 (2005).

13. R. D. Shannon and C. T. Prewitt, *Acta Crystallogr. Sect. B: Struct. Cryst.* **B 25**, 925-946 (1969).

14. S. McIntosh, J. F. Vente, W. G. Haije, D. H. A. Blank, and H. J. M. Bouwmeester, *Chem. Mat.* **18**, 2187-2193 (2006).

15. J. K. Fink, *J. Nucl. Mater.* **279**, 1-18 (2000).

16. A. Nakajima, A. Yoshihara, and M. Ishigame, *Phys. Rev. B* **50**, 13297-13307 (1994).

17. J. B. Wachtman, M. L. Wheat, H. J. Anderson, and J. L. Bates, *J. Nucl. Mater.* **16**, 39-& (1965).

18. P. M. Macedo, W. Capps, and J. B. Wachtman, *J. Am. Ceram. Soc.* **47**, 651-651 (1964).